

Emergent Potts order in the kagomé $J_1 - J_3$ Heisenberg model

Vincent Grison,¹ Pascal Viot,^{1,*} Bernard Bernu,^{1,†} and Laura Messio^{1,2,‡}

¹*Sorbonne Université, CNRS, Laboratoire de Physique Théorique de la Matière Condensée (LPTMC), F-75005 Paris, France*

²*Institut Universitaire de France (IUF), 1 rue Descartes, F-75005 Paris, France*

(Dated: August 3, 2020)

Motivated by the physical properties of Vesignieite $\text{BaCu}_3\text{V}_2\text{O}_8(\text{OH})_2$, we study the $J_1 - J_3$ Heisenberg model on the kagomé lattice, that is proposed to describe this compound for $J_1 < 0$ and $J_3 \gg |J_1|$. The nature of the classical ground state and the possible phase transitions are investigated through analytical calculations and parallel tempering Monte Carlo simulations. For $J_1 < 0$ and $J_3 > \frac{1+\sqrt{5}}{4}|J_1|$, the ground states are not all related by an Hamiltonian symmetry. Order appears at low temperature via the order by disorder mechanism, favoring colinear configurations and leading to an emergent $q = 4$ Potts parameter. This gives rise to a finite temperature phase transition. Effect of quantum fluctuations are studied through linear spin wave approximation and high temperature expansions of the $S = 1/2$ model. For J_3 between $\frac{1}{4}|J_1|$ and $\frac{1+\sqrt{5}}{4}|J_1|$, the ground state goes through a succession of semi-spiral states, possibly giving rise to multiple phase transitions at low temperatures.

I. INTRODUCTION

The existence of competing interactions in a magnetic spin lattice model leads to the inability to satisfy all pair interactions simultaneously. The system is said to be *frustrated*. While its effects in a classical spin model can be important, they are enforced for quantum spin models, where they may induce spin liquid ground states¹. These phases break none of the Hamiltonian symmetries and as a consequence, show no magnetic long range order. Thus, it is interesting to pick up classical models where frustration has the largest effects, in view to detect quantum models hosting highly disordered phases.

Such spin models on the bidimensional kagomé lattice have a long history, both from theoretical and experimental point of view. The most studied model is definitely the first neighbor antiferromagnet, realized in Herbertsmithite², even if impurities and other interactions keep this compound away from its idealization. In the search of the perfect chemical realization of this specific model, many other kagomé compounds were proposed, such as Kapellasite³, Volborthite⁴, Haydeite^{5,6}, Ba-Vesignieite⁷⁻¹⁰, Sr-Vesignieite¹¹... although they were finally described by different interactions. Here we shall restrict our attention to the model supposed to describe the Ba-Vesignieite compound¹², with small first neighbor ferromagnetic and large third neighbor antiferromagnetic interactions.

In the Vesignieite $\text{BaCu}_3\text{V}_2\text{O}_8(\text{OH})_2$ compound, magnetic Cu atoms form decoupled and perfect bidimensional kagomé layers of $S = 1/2$ spins. Its Curie-Weiss temperature is around -77K ⁷, indicating an antiferromagnetic dominant coupling that was first proposed to be first neighbor⁷. Moreover, specific heat, magnetic susceptibility and powder neutron diffraction measurements on Vesignieite were supporting the spin liquid ground state hypothesis^{7,13}, even if more and more indications of a phase transition around 9K appeared with time^{13,14}. This transition, probably related to a small interlayer

coupling, is now clearly identified in crystalline samples⁸. Finally, neutron diffraction results on crystals¹³ indicated that the short range spin correlations were uncompatible with antiferromagnetic first neighbor interactions (J_1 in Fig. 1), but coherent with a dominant third neighbor interaction J_3 . These unusual interactions in Ba-Vesignieite are our main motivation to explore this kagome model. To the best of our knowledge, the $J_1 - J_3$ Heisenberg model on the kagomé lattice¹² has still not been studied for large J_3 .

In Heisenberg models, the interaction between two tridimensional unit spins on sites i and j is given by $J_{i,j} \mathbf{S}_i \cdot \mathbf{S}_j$. $J_{i,j}$ is the coupling constant, either positive for antiferromagnetic interactions, or negative for ferromagnetic ones. Unfrustrated classical Heisenberg models have colinear ground states (i.e. all the spins are oriented along a unique line, with only two possible directions). It is notably the case for ferromagnetic models, or for antiferromagnetic ones on bipartite lattices, where sites can be labelled A or B in such a way that only different types of sites interact. Frustration can induce non-colinear magnetic orders, as on the triangular lattice with antiferromagnetic interactions: three sublattices A , B and C host spins directions \mathbf{S}_A , \mathbf{S}_B and \mathbf{S}_C each at an angle of 120° from the others. In this case, spins are no more colinear but remain coplanar. More rarely, non-coplanar spin states are obtained in Heisenberg models^{3,15-18}, with possibly large unit cells. Twelve-site unit cells, with spins pointing towards the corners of a cuboctahedron are for example obtained on the kagomé lattice for interactions up to third neighbors^{3,15,16}.

The Mermin-Wagner theorem states that no continuous symmetry of a Hamiltonian can be broken at finite (non-zero) temperature in two dimensions¹⁹⁻²¹. Yet, other types of finite temperature phase transitions exist, relating phases with or without symmetry breaking^{22,23}, associated with topological defects for instance. When a Hamiltonian symmetry is broken, the Mermin-Wagner theorem implies that it is a discrete one. In Heisen-

berg models, global spin rotations form a continuous symmetry group, thus the broken symmetry is different: it can be a lattice symmetry²⁴, or the time reversal symmetry^{25,26}. In most cases, a phase transition can be inferred from the analysis of the ground state manifold: several connected components generally correspond to a broken discrete symmetry. For example, if the spins are non coplanar, the ground state manifold is isomorphic to $O(3)$, which has two connected components $\pm SO(3)$. An emergent Ising parameter ± 1 (chirality) can be defined, indicating in which connected component the spin state is. The time reversal symmetry ($\mathbf{S}_i \rightarrow -\mathbf{S}_i$) is broken in the ground state but is restored at finite temperature via a phase transition^{15,25,26}.

In most cases, all the ground states are equivalent, in the sense that they are related by a symmetry of the Hamiltonian. For example, two ground states of the triangular antiferromagnetic lattice each have three different spin orientations on their sublattices: \mathbf{S}_A , \mathbf{S}_B , \mathbf{S}_C and \mathbf{S}'_A , \mathbf{S}'_B , \mathbf{S}'_C . But there exists a three dimensional rotation R such that

$$\forall \alpha \in \{A, B, C\}, \mathbf{S}'_\alpha = R \mathbf{S}_\alpha.$$

R is an Hamiltonian symmetry: for any spin configuration, the R -transformed one has the same energy. When the symmetries of the Hamiltonian fail to make all of the ground states equivalent, we speak of accidental degeneracy. Different ground states then have different properties, including different density of low energy excitations. This implies that, at low temperatures, some of the ground states are selected by the *order by disorder* mechanism. A connected manifold of ground states can thus be reduced to disconnected components at infinitesimal temperatures, possibly giving rise to phase transitions with an emergent discrete order parameter. It is precisely what occurs in some part of the phase diagram of the $J_1 - J_3$ kagomé Heisenberg model, and is the subject of this article.

The paper is organized as follows. In Sec. II, we present the model and its classical ground states. In Sec. III A, the known examples of order by disorder-induced phase transitions are detailed. Sec. III is first devoted to a discussion of the octahedral phase found in the range of parameters corresponding to the Ba-Vesignieite compound (Sec. III A), leading in a second part to the definition of an appropriate order parameter (Sec. III B), opening the possibility of a related phase transition. The finite temperature phase diagram of the classical model is explored using parallel tempering Monte Carlo simulations in Sec. IV and thermal linear spin wave calculations in Sec. V A. A phase transition is evidenced through a finite size analysis, and the critical exponents are numerically evaluated. The effects of quantum fluctuations are discussed through a linear spin wave approximation (Sec. V B) and high temperature series expansions (Sec. VI). The relevance of our approach in the case of the $S = 1/2$ Ba-Vesignieite compound is discussed. In conclusion (Sec. VII), the nature of the phase transi-

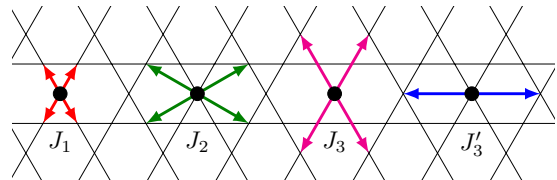


FIG. 1. Sketch of first, second and third neighbor interactions on the kagomé lattice, J_1, J_2, J_3 and J'_3 respectively. The third neighbor interaction is split in two contributions: J'_3 corresponds to interactions between spins located on two opposite corners of an hexagon, and J_3 between spins located at the same distance, but on corners of two adjacent hexagons.

tion experimentally observed in Vesignieite is discussed in light of the numerical and analytical results.

II. THE MODEL AND ITS $T = 0$ CLASSICAL PHASE DIAGRAM

The kagomé lattice consists of triangles sharing corners, with three sites per unit cell (see Fig. 1). On each site i , we place a unit vector \mathbf{S}_i called spin (in the quantum model, they are $S = 1/2$ spins). For our study, we consider spin interactions between first and third neighbors, with respective strengths J_1 and J_3 (Fig. 1). The Hamiltonian of the system reads:

$$\mathcal{H} = J_1 \sum_{\langle i, j \rangle} \mathbf{S}_i \cdot \mathbf{S}_j + J_3 \sum_{\langle i, j \rangle_3} \mathbf{S}_i \cdot \mathbf{S}_j, \quad (1)$$

where the sums over $\langle i, j \rangle$ and $\langle i, j \rangle_3$ indicate a sum over all first and third neighbor links of the lattice.

Let us first investigate the landscape of possible ground states, presented in Fig. 2. We define an energy scale $J = \sqrt{J_1^2 + J_3^2}$ and an angle ϕ such that $(J_1, J_3) = (J \cos \phi, J \sin \phi)$.

The actual determination of the ground state(s) for given (J_1, J_3) is a tough problem. No general procedure is known for a classical Hamiltonian such as ours, outside of the case of a quadratic Hamiltonian on a Bravais lattice, that can be handled by the Luttinger-Tizsa (LT) method²⁷. This method can still be applied in the other cases, but then only gives a lower bound for the ground state energy (see App. A). If the energy of a trial state reaches this lower bound, it is then proved to be a ground state. Using a group-theoretical approach, a set of spin configurations called *regular magnetic orders* were defined¹⁷, that are important trial states. In our case, regular magnetic orders are ground states for almost the whole phase diagram, with the exception of a small transition region (grey area of Fig. 2).

We now describe the the phase diagram of Fig. 2, whose most phases are described on Fig. 3. When both J_1 and J_3 are negative, the ground state is obviously a ferromagnetic state, which survives for small positive J_3 . Moving on to an antiferromagnetic coupling $J_1 > 0$,

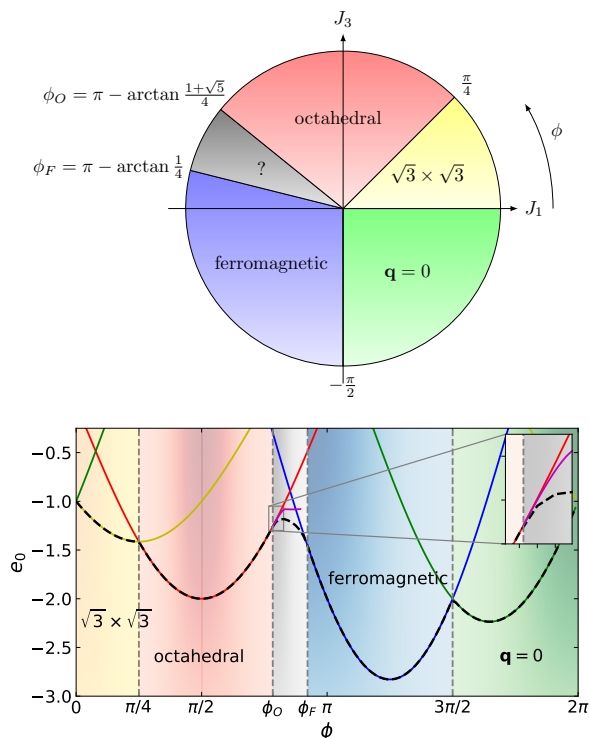


FIG. 2. Top: Ground states in the $J_1 - J_3$ plane (see Fig. 1 for the definition of J_1 and J_3). The different orders are described in Fig. 3. Bottom: Energy per site e_0 for each state named above, and LT lower bound (dashed). $e_0 = 2J_1 + 2J_3$ for the ferromagnetic state (blue line), $-2J_3$ for the octahedral state (red), $-J_1 + 2J_3$ for the $\mathbf{q} = 0$ state (green) and $-J_1 - J_3$ for the $\sqrt{3} \times \sqrt{3}$ state (yellow). The lower bound is reached everywhere except in the grey region. The magenta curve is the energy of the variational ground state, described in the text and in Fig. 5.

we encounter the kagomé Heisenberg antiferromagnet for $J_3 = 0$. This model is known for its extensive ground-state degeneracy, which is lifted when J_3 is switched on: $J_3 < 0$ aligns spins equivalent under translations of the lattice in different triangles, giving rise to the $\mathbf{q} = 0$ phase, while $J_3 \gtrsim 0$ leads to the $\sqrt{3} \times \sqrt{3}$ order, which survives up to $J_3 = J_1$ ($\phi = \pi/4$).

If $J_1 = 0$, the lattice is decoupled into three square sublattices (Fig. 4), each ferromagnetically ($J_3 < 0$) or antiferromagnetically ($J_3 > 0$) ordered, in three independent spin directions. When $J_3 < 0$, an infinitesimal (positive or negative) J_1 completely lifts the degeneracy towards the ferromagnetic or $\mathbf{q} = 0$ states previously discussed, but this is not the case for $J_3 > 0$. To see why, it is useful to consider a single spin and its nearest neighbors. The large value of J_3 imposes that each spin is surrounded by pairs of anti-aligned spins, thus *cancelling out* nearest-neighbor energetic contributions as long as each sublattice stays ordered (Fig. 4). Thus, a small, arbitrary, J_1 does not lift the degeneracy at $T = 0$. Among the degen-

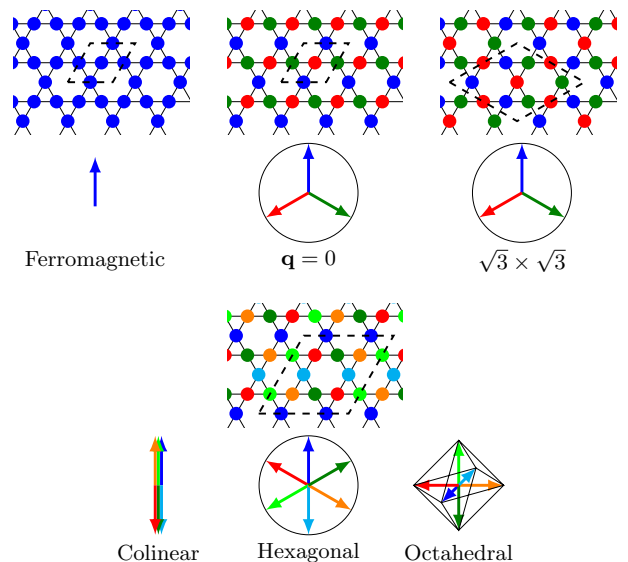


FIG. 3. Top: Three long-range orders on the kagomé lattice, that are ground states in some part of the phase diagram of Fig. 2. Bottom: Colinear, hexagonal and octahedral states, that belong to the ground state manifold of the octahedral phase of Fig. 2.

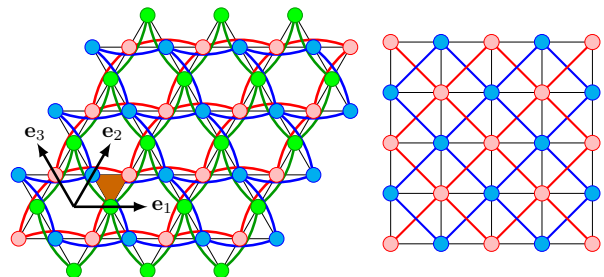


FIG. 4. Left: When only J_3 interactions are present, the kagomé lattice divides into three independent deformed square lattices (with blue, red and green sites and links). When $J_3 > 0$, an antiferromagnetic $T = 0$ spin order sets in on each sublattice, with an arbitrary direction. A small J_1 does not lift this degeneracy as it couples for example a red spin with two opposite green spins and two opposite blue spins. The same phenomena occurs on the $J_1 - J_2$ square lattice for a strong AF J_2 (right).

erate configurations in this manifold (some of them are illustrated in Fig. 3), we find a regular order whose spin directions correspond to the vertices of an octahedron, hence the name *octahedral order*¹⁷. At stronger J_1 , the octahedral state breaks down in favor of other states - $\sqrt{3} \times \sqrt{3}$ for $J_1 > 0$, and a succession of unconventional states with eventually several wave vectors for $J_1 < 0$, before reaching the ferromagnetic sector again.

We will now briefly discuss the unconventional ground states of Fig. 2, even if a detailed description is under the scope of this article. In this area of the phase diagram,

the LT lower bound of the energy is not reached by any spin configuration and the system has to find a compromise between the different wave vectors to minimize its energy. This situation occurs as soon as the wave vector \mathbf{q}_{\min} corresponding to the lowest eigenvalue $\lambda_{\min}(\mathbf{q})$ becomes different from those of the simple neighboring phases. When ϕ decreases from π , we leave the ferromagnetic state at $\phi_F = \pi - \arctan \frac{1}{4}$. The only \mathbf{q}_{\min} , previously the zero wave vector, splits into six \mathbf{q}_{\min} staying on lines going from the center of the BZ to its corners. When ϕ increases, departing from $\pi/2$, we leave the octahedral state at $\phi_O = \pi - \arctan \frac{1+\sqrt{5}}{4} \simeq 0.78\pi$ (proof in App. C, see also Fig. 17). The three \mathbf{q}_{\min} previously at the middles of the edges of the BZ split into six \mathbf{q}_{\min} staying on lines going from the middles of the edges of the BZ to its center. This part of the phase diagram is very rich. No method exists to determine the ground states, which usually break several symmetries of the Hamiltonian. As an example, we describe here the ground state found near ϕ_O , which is similar to the alternating conic spiral state of¹⁸ and whose energy is given in Fig. 2. From numerical simulations (iterative minimization¹⁸), it appears that one of the three sublattices of Fig. 4 develops spin orientations in a plane, say the xy plane, whereas the other two form a cone of axis z and of small angle ϕ (see Fig. 5). Note that the orientations of the two last sublattices are exactly the same, translated by a lattice spacing. Thus, this state is a spiral state, in the sense given in¹⁷, but with an enlarged unit cell of twelve sites, reminiscent of the parent octahedral state.

III. GROUND STATE SELECTION IN THE OCTAHEDRAL PHASE

A. Order by disorder

When $J_1 = 0$, the three sublattices of Fig. 4 are independent and each of them develops its own long range order at zero temperature. The ground state is then fully determined by the orientation on three reference sites (say the three sites of a reference unit cell): an element of \mathcal{S}_2^3 , where \mathcal{S}_2 is the unit sphere in three dimensions. The effect of a small J_1 depends on the sign of J_3 , as detailed in Sec. II. For a negative J_3 , no accidental degeneracy survives to an infinitesimal J_1 , whatever its sign. On the other hand, for positive J_3 , an infinitesimal J_1 has no effect on this degeneracy whatever its sign. Note that this accidental degeneracy is not extensive, i.e. does not increase with the lattice size. When temperature or quantum fluctuations are switched on, the phenomena of order by disorder occurs, lifting this degeneracy to a subset of \mathcal{S}_2^3 - which will be determined below to be $\mathcal{S}_2 \times K_4$, where K_4 is the Klein four-group.

Before considering in more detail the kagomé $J_1 - J_3$ model, let us list some models where such (simpler) accidental degeneracies are known. Historically, the order by disorder (ObD) phenomenon was described by Vil-

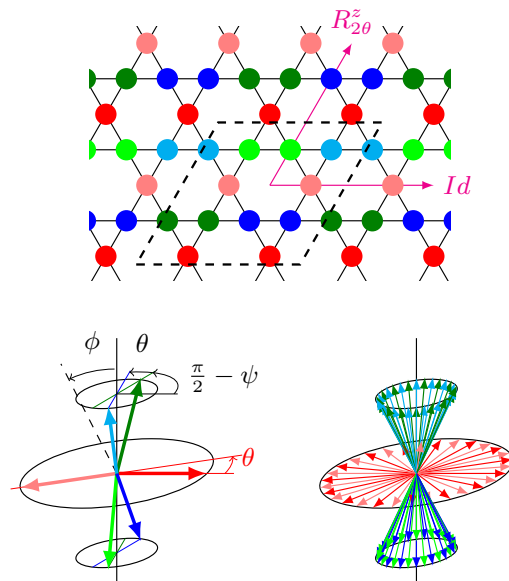


FIG. 5. Spin configuration supposed to be the ground state for ϕ slightly larger than ϕ_O , i.e. in the unconventional phase of Fig. 2. The spins of the dashed unit cell of 12 sites have 6 orientations, as indicated on the bottom left. The parametrization of this state is detailed in App. C. A translation in the \mathbf{e}_1 direction let the spins invariant, whereas in the \mathbf{e}_2 direction, they are rotated by 2θ around the z axis. Bottom right: orientation of the spins over the full lattice.

lain et al. on a domino model of Ising spins²⁸. For a Heisenberg model, the most spectacular and most studied example of ObD is without any doubt the kagomé antiferromagnet²⁹⁻³⁷, whose degeneracy is extensive, as for the domino model. On the kagomé lattice, thermal or quantum ObD selects coplanar states, whose number is still extensive, giving rise to possible further ObD effects, such as those occurring in the octupolar order.

We now focus our attention on other cases of bidimensional lattices, which share with the $J_1 - J_3$ kagomé model a non-extensive accidental degeneracy, with a continuous set of ground states. This situation is relatively common for Heisenberg Hamiltonians with nearest and next-nearest neighbor interaction. A well studied case is the $J_1 - J_2$ Heisenberg model on a square lattice^{38,39}, where in the case of strong AF J_2 , the lattice decouples into 2 sublattices with independent antiferromagnetic orders (\mathcal{S}_2^2 ground state manifold), see Fig. 4, right. Both thermal and quantum fluctuations favor collinear ordering, the ground state manifold being reduced to $\mathcal{S}_2 \times \mathbb{Z}_2$: the first sublattice has a free orientation (\mathcal{S}_2) and the second one can align its reference spin with the one of the first sublattice, or set it opposite (\mathbb{Z}_2). The effective set of ground states is now formed by two disconnected manifolds. Depending on the discrete component selected by the system, the $T \rightarrow 0^+$ order is an horizontal or vertical columnar state. This emergent Ising variable gives rise to a phase transition at finite temperature, compatible

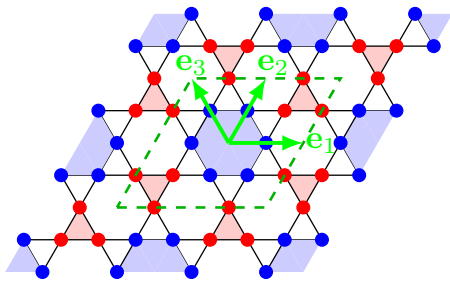


FIG. 6. In the octahedral phase of Fig. 2, order by disorder effect tends to align along a unique direction the spins of the three antiferromagnetic square lattices depicted in Fig. 4. The resulting colinear spin order has a unit cell of 12 sites (in dashed green) and only two opposite spin orientations (on the blue and red sites).

with the Mermin-Wagner theorem.

The Heisenberg models on triangular⁴⁰ and honeycomb⁴¹ lattices also develop ObD favoring colinear states (with a $\mathcal{S}_2 \times \mathbb{Z}_3$ effective set of ground states) for some values of the $J_1 - J_2 - J_3$ exchanges. But contrary to the square lattice, no limit of decoupled lattices allows for a simple understanding of this phenomenon. In the presence of a magnetic field, there are also many examples of ObD, where colinear configurations are stable and lead to magnetization plateaus^{42,43}.

For the octahedral phase of the $J_1 - J_3$ kagomé lattice, we can infer from the $J_1 - J_2$ square lattice that the three sublattices align their spins colinearly under thermal or quantum fluctuations. The ground state manifold thus changes from \mathcal{S}_2^3 to $\mathcal{S}_2 \times K_4$: the first sublattice has a free orientation (\mathcal{S}_2), the second and third ones can align its reference spin with the one of the first sublattice, or set it opposite (fixing an element of K_4) (see Fig. 6). The choice of a reference spin for each sublattice is arbitrary, which suggests to use K_4 as the symmetry group labelling the different connected components, instead of the isomorphic \mathbb{Z}_2^2 , since all symmetries are then explicitly treated on the same footing. Note also that the point-group symmetry of the lattice is unchanged - only the translational symmetries are broken. K_4 is an unusual broken symmetry, but it has already been reported for example in an interacting electron model on the honeycomb lattice⁴⁴.

The (effective) ground-state manifold is sometimes abusively called the *order parameter space*. We take care here to distinguish them, as an order parameter taking values in another set will be defined in the coming section.

B. Definition of an order parameter

It was envisaged in the preceding section that the ground-state manifold \mathcal{S}_2^3 effectively reduces down to $\mathcal{S}_2 \times K_4$ when infinitesimal temperatures are considered,

i.e. when states in the limit $T \rightarrow 0^+$ are considered. We construct in this section a local order parameter Σ for the case at hand, that will be averaged over the full lattice, a non-zero value in the thermodynamical limit revealing an ordered, symmetry breaking phase. We recall here that several order parameter definitions are possible, and that specific order-parameters are required for different broken symmetry.

When each local configuration can easily be associated with a ground-state, the order-parameter can take values in the ground state manifold, under some conditions on the broken symmetry, discussed below. This is the case for the local magnetization of ferromagnetic Ising or Heisenberg models, for example, where the order parameter is defined on each lattice site as the spin orientation, or for the alternated magnetization of Néel orders. In these cases, the order parameter takes values in \mathcal{S}_2 and can reveal a \mathcal{S}_2 symmetry breaking (at $T = 0$, or in 3 dimensions for example).

Complications arise when the definition of a ground-state involves several sites, with constraints on the spin orientations. The antiferromagnetic triangular lattice is such an example: the sum of 3 spins of a triangle is zero at $T = 0$, and the orientation of two non colinear spins are required to fully determine a ground state. This ground-state manifold is homeomorph to $SO(3)$ ⁴⁵. For $T \neq 0$, the constraint on the sum of spins is no more verified and there is no direct way to chose a ground state related to this configuration. We are here quite lucky, as a local configuration on a triangle of the kagome lattice can uniquely be propagated over the full lattice to form a state of the octahedral phase. A first possible order parameter is such a triplet of unit spins, forming an element of \mathcal{S}_2^3 . However, \mathcal{S}_2^3 as order parameter space does not do the job to reveal a possible symmetry breaking. The Mermin-Wagner theorem states that continuous symmetries are unbroken at finite temperature. Here, there are the global spin rotations $SO(3)$. Thus $SO(3)$ forms classes of equivalence in \mathcal{S}_2^3 such that at infinitesimal temperature, spin waves disorder the ground state and disperse the local order parameter over the full equivalence class, when measured over the full lattice. Each such class has a zero average in \mathcal{S}_2^3 , which rules out \mathcal{S}_2^3 as order-parameter space to detect any finite temperature phase transition.

Thus we are forced to use a $SO(3)$ invariant description of the ground-state manifold, as the quotient $\mathcal{S}_2^3/SO(3)$, in order to appropriately account for the possible symmetry breakings. Each point in \mathcal{S}_2^3 is defined by 6 parameters, while $SO(3)$ is a tridimensional manifold, from which we deduce that $\mathcal{S}_2^3/SO(3)$ has dimension 3 as well. Points in this space, equivalence classes of states, must be described using $SO(3)$ invariants built from the initial variables $(\mathbf{S}_A, \mathbf{S}_B, \mathbf{S}_C)$ on a triangle ABC . An obvious choice is to use the dot product, which immediatly provides us with three invariants, that we group in a *vector* $\sigma(\mathbf{S}_A, \mathbf{S}_B, \mathbf{S}_C) = (\mathbf{S}_B \cdot \mathbf{S}_C, \mathbf{S}_C \cdot \mathbf{S}_A, \mathbf{S}_A \cdot \mathbf{S}_B)$. The image of σ is a subset of \mathbf{R}^3 , whose shape is a slightly

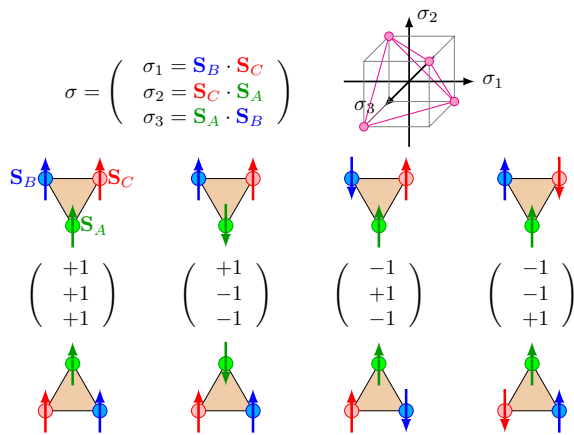


FIG. 7. Four possible spin configurations for $T \rightarrow 0^+$ on a reference triangle of the kagomé lattice (up to a global spin rotation). They are labeled by a triplet of spin dot products σ and stay on the vertices of a tetrahedron.

inflated tetrahedron. Its vertices correspond to colinear configurations, with three ± 1 vector components, and it can be shown that this shape indeed has the tetrahedral group T_d as its symmetry group. Note that we have lost the distinction between time-reversed spin configurations $\mathbf{S}_i \rightarrow -\mathbf{S}_i$. Points in the image of σ have one class of pre-images when the three spins are coplanar (as spin inversion is equivalent to a rotation of π in this case), two when they are not. Thus, σ is unable to describe the breaking of the \mathbb{Z}_2 inversion subgroup of the $O(3)$ global spin transformations.

Returning to ObD, the alignment of all spins can now be easily identified using σ . The tendency to colinearity of neighboring spins can be visualized as free energy barriers effectively pushing the ground-state configurations towards the vertices of the inflated tetrahedron, points of high symmetry, describing perfect (anti)-alignment in spin triplets. By considering vertices only, one can quickly observe that each vertex is invariant under the permutation of the three others, \mathcal{S}_3 , while the whole symmetry group is isomorphic to the permutation group of four points \mathcal{S}_4 . Consequently, our points may be described as the quotient space $\mathcal{S}_4/\mathcal{S}_3 \simeq K_4$, a genuine group since \mathcal{S}_3 is normal in that case. This group provides the set of transformations that allows us to navigate between the different colinear ground states, by flipping pairs of spins (or not flipping any for the neutral element), and is thus the actual symmetry broken by this phase transition - they simply represent the action of translations of the lattice on a ground state. As a time-reversal spin transformation ($\mathbf{S}_i \rightarrow -\mathbf{S}_i$) let the elements of this group invariant, the impossibility to distinguish states breaking this symmetry, evocated above, does not evince σ as an appropriate order parameter.

Up to now, we have considered a single reference triangle ABC . Depending on the choice of the labels A , B and C of the triangle vertices (4 possibilities), σ under-

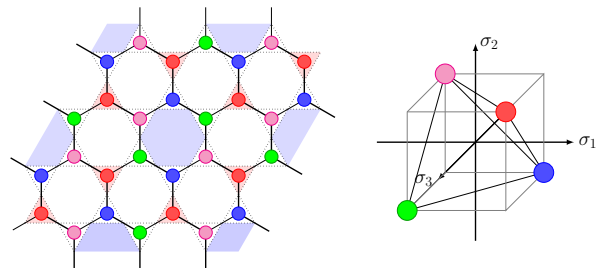


FIG. 8. Lattice of effective spins, i.e. values of the tridimensional order parameter locally defined on each triangle. Shared vertices between triangles are represented as edges linking the corresponding sites. Each color corresponds to a value a given value of σ , as shown on the right panel.

goes a transformation. To fix the definition of σ , its i th component σ_i is defined as the dot product of spins on a link directed along the vector \mathbf{e}_i of Fig. 6. This unambiguously defines σ on all the pointing-down as well as pointing up triangles (see Fig. 7).

The four possible triplets for colinear configurations are represented on Fig. 7. The centers of up and down triangles on the kagomé lattice form a honeycomb lattice, and σ is an effective (non unit) spin on these sites, oriented alternately as indicated on Fig. 8 in a colinear ground state configuration. Note that once σ is chosen on one of the kagomé triangle in a colinear ground state configuration (or equivalently on one of the honeycomb lattice sites), σ on any other triangle can be deduced from elementary operations belonging to the Klein group K_4 : an \mathbf{e}_i translation of the spins rotates σ by π around the σ_i axis. The tetrahedra of σ orientations falls in one of four possible orientations, corresponding to a $q = 4$ Potts variable⁴⁶.

By analogy with the alternate order parameter used for antiferromagnetic long-range order, we define an alternate order parameter Σ , homogeneous over the full lattice. The evolution of its average over the full lattice as a function of the temperature and of the system size will now be studied below using Monte Carlo simulations. Note that in a colinear ground state, Σ is homogeneous, and only four ground states are possible. In this aspect, the effective model for the Σ variables resembles more to the ferromagnetic $q = 4$ Potts model than to the antiferromagnetic one, whose degeneracy on the honeycomb lattice would be extensive.

IV. MONTE CARLO SIMULATIONS AT FINITE TEMPERATURE

A. The method

To investigate the phase diagram of the $J_1 - J_3$ model, we perform Monte Carlo simulations by implementing a parallel-tempering method⁴⁷. In the case of first-

order phase transitions, this method enables to overcome the associated free-energy barriers by considering N_p replicas of the system at different temperature T_i , with $i = 1, \dots, N_p$. Each replica constitutes a separate, parallel, simulation box whose state evolves independently via local spin updates, but can also periodically be swapped with that of its immediate neighbors. Hence, higher temperature simulation boxes allow lower temperature ones to sample their phase space much more efficiently. The temperature interval is chosen in order to cover the region where a putative phase transition is expected, and the difference of inverse temperature between two adjacent replicas $\Delta\beta$ is kept constant (we also tried a geometric progression for the inverse temperatures in the range, without noticing significant changes for the convergence of the method).

In order to satisfy a detailed balance for this process, the probability P_{PT} of accepting an exchange of configurations between boxes i and $i + 1$ is chosen with a Metropolis rule

$$P_{PT}(i \leftrightarrow i + 1) = \text{Min}(1, \exp(\Delta\beta\Delta E)), \quad (2)$$

with $\Delta\beta = \beta_i - \beta_{i+1}$ and $\Delta E = E_i - E_{i+1}$. The double arrow means that the probability P_{PT} is symmetric to the reverse exchange.

The mean acceptance probability $P_A(i \leftrightarrow i + 1)$ between boxes i and $i + 1$ is the average of $P_{PT}(i \leftrightarrow i + 1)$ over thermalized configurations, and writes:

$$P_A(i \leftrightarrow i + 1) = \int dE_i dE_{i+1} P_{\beta_i}(E_i) P_{\beta_{i+1}}(E_{i+1}) P_{PT}(i \leftrightarrow i + 1), \quad (3)$$

where $P_{\beta_i}(E_i)$ denotes the equilibrium probability of the box i to have an energy E_i . Eq. (3) is merely a weighted sum over all possible energetic configurations for two given neighboring boxes. In order to optimally schedule the temperatures, we check that the acceptance probability of swaps between neighboring replicas is near 0.5⁴⁷.

We choose an even number of replicas N_p and at constant time intervals, two kinds of exchanges between neighboring boxes are proposed: either exchanges between all pairs $(2k - 1, 2k)$ where $k = 1, \dots, N_p/2$ or exchanges between all pairs $(2k, 2k + 1)$ where $k = 1, \dots, N_p/2 - 1$, which preserves the ergodicity of the process. Otherwise, we perform local updates of spins for each simulation box according to a Metropolis rule.

In simulations on a lattice of size L , we store the histograms of the energy and of the order parameter modulus $|\sum_{\nabla, \Delta} \Sigma|$ for each temperature, giving directly access to the mean energy $\langle E \rangle(\beta, L)$, and the mean Potts magnetization $\langle \Sigma \rangle(\beta, L)$. The specific heat C_V , the susceptibility of the order parameter χ_Σ , and the associated

Binder parameter B_Σ are given per lattice site as:

$$C_V(\beta, L) = \frac{\beta^2}{N} (\langle E^2 \rangle - \langle E \rangle^2) \quad (4a)$$

$$\chi_\Sigma(T, L) = N(\langle \Sigma^2 \rangle - \langle \Sigma \rangle^2) \quad (4b)$$

$$B_\Sigma(\beta, L) = 1 - \frac{\langle \Sigma^4 \rangle}{3\langle \Sigma^2 \rangle}. \quad (4c)$$

Moreover, by using the reweighing method⁴⁸, and the histograms obtained in simulations, one builds for each box i all estimated above quantities within a temperature interval $[(\beta_i + \beta_{i-1})/2, (\beta_i + \beta_{i+1})/2]$. Collecting all curves, one can build a global graph from T_{\min} to T_{\max} . The convergence for all temperatures of the parallel tempering method is confirmed when the curve is continuous at each boundary between two temperature intervals.

In order to perform a finite scaling analysis, we simulated different system sizes of the kagomé lattice with periodic boundary conditions. L is the linear size of the lattice, and the number of sites is $N = 3L^2$. By using simulation data, we determine the maxima $C_V^{\max}(L)$ and $\chi_\Sigma^{\max}(L)$ of these quantities, occurring at temperatures $T_c^{C_V}(L)$ and $T_c^{\chi_\Sigma}(L)$. For a continuous phase transition, the finite size scaling at the lowest order of these quantities is given by:

$$C_V^{\max}(L) \simeq aL^{\alpha/\nu} + b, \quad (5a)$$

$$\chi_\Sigma^{\max}(L) \simeq cL^{\gamma/\nu} + d, \quad (5b)$$

$$T_c^{C_V, \chi}(L) \simeq eL^{-1/\nu} + T_c(\infty), \quad (5c)$$

where α , ν and γ are critical exponents whose values for the ferromagnetic $q = 4$ Potts model are recalled in App. B and $T_c(\infty)$ is the critical temperature of the phase transition. For a first-order phase transition, the finite size scaling is given by:

$$C_V^{\max}(L) \simeq aL^2 + b, \quad (6a)$$

$$\chi_\Sigma^{\max}(L) \simeq cL^2 + d, \quad (6b)$$

$$T_c^{C_V, \chi}(L) \simeq eL^{-2} + T_c(\infty). \quad (6c)$$

B. Results for ferromagnetic J_1

The linear size of the lattice L goes from 12 to 104. The interaction between nearest neighbors J_1 is set to -1 and J_3 is varied from 0.2 to 2. By considering the $T = 0$ phase diagram (top of Fig. 2), this corresponds to a vertical line in the upper left quarter, which intersects three ground state sectors: ferromagnetic, unconventional and octahedral. One leaves the ferromagnetic phase when $J_3 = \frac{1}{4}$ and enter the degenerate octahedral phase for $J_3 = \frac{1+\sqrt{5}}{4} \simeq 0.809$, where one expects a finite temperature phase transition due to emergence of the discrete K_4 order parameter. Note that the table IV B gives an one-to-one mapping between the coupling ratio

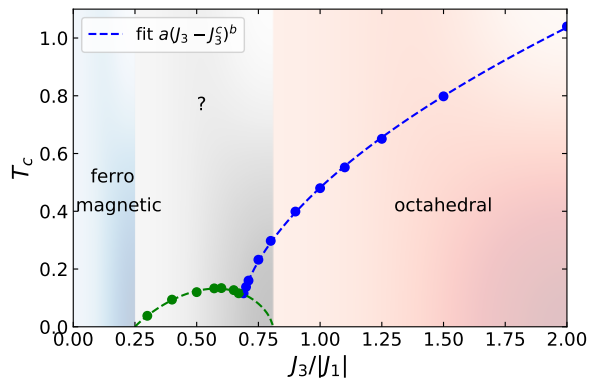


FIG. 9. Phase diagram of the $J_1 - J_3$ Heisenberg model on the kagomé lattice. A phase transition with both C_V and χ_Σ divergency (blue points) is evidenced by Monte Carlo classical simulations, restoring the K_4 symmetry. The dashed blue line is a 3-parameter fit with a power law: $a = 0.88$, $b = 0.56$, $J_3^c = 0.66$. Green points are phase transitions with no χ_Σ divergency. The green dashed line is a guide to the eyes.

$J_3/ J_1 $	ϕ/π	$J_3/ J_1 $	ϕ/π	$J_3/ J_1 $	ϕ/π
0	1	0.68	0.810	1	3/4
0.25	0.922	0.75	0.795	2	0.648
0.5	0.852	0.809	0.783	∞	1/2

TABLE I. $J_3/|J_1|$ versus ϕ for $J_1 = -1$. $\phi_F \simeq 0.922\pi$ and $\phi_O \simeq 0.783\pi$ are the boundaries of the unconventional phase, whose exact value is given in Fig. 2.

$J_3/|J_1|$ and the parameter ϕ introduced in the preceding section.

C_V and/or χ_Σ shows an maximum increasing with L for some J_3 values, revealing a phase transition. The resulting finite temperature phase diagram is displayed in Fig. 9. Blue points indicate both a C_V and χ_Σ divergency, whereas green points indicate that only C_V diverges.

We now discuss in more detail our results by considering the three different regions (ferromagnetic, unconventional and octahedral ground states).

1. Ferromagnetic region: no transition

For $J_3 = 0.2$ (let us recall that J_1 is set to -1 in simulations), no phase transition was observed, at any temperature. There is no evolution of the specific heat with the system size. Hence our results are in line with the predictions of the Mermin-wagner theorem for this phase, as expected.

2. Non K_4 phase transitions in the unconventional phase

When $0.25 < J_3 < 0.809$, the ground state is not easily determined and seems to be very dependent of J_3 , as explained in Sec. II (for example, with a succession of various types of wave vectors). The following values of J_3 have been explored: 0.3, 0.4, 0.5, 0.6, 0.65, 0.67, 0.69, 0.7, 0.71, 0.75, 0.8, all showing a unique divergency of $C_V(\beta, L)$ with L .

For $0.25 \leq J_3 \leq 0.67$, the K_4 Potts parameter Σ remains close to zero at all temperatures. However, the specific specific heat displays a peak at low temperature, whose size increases with L . The approximative limit of T_{C_V} when L increases seems to be a continuous function of L and is indicated as green points on Fig. 9: it increases from zero for $J_3 = 1/4$ up to $T_c = 0.134(1)$ for $J_3 \simeq 0.60(3)$, and slightly decrease down to $0.116(1)$ up to $J_3 = 0.67(2)$. Due to the nature of the ground state, it is possible that transitions associated with various broken symmetries occur in this range of parameters. It is for example probable that the three-fold spatial rotation is broken at low T for $J_3 \simeq 0.67$ as the order of Fig. 5 particularizes one of the three sublattices. We did not try to identify the order parameter associated with these phase transitions as the focus of this study is the octahedral phase.

For $0.6 \leq J_3 \leq 0.67$, the mean energy per site at low T depends on the system size even quite far from the critical temperature. Moreover the temperature of C_V^{\max} varies non monotonously with the system size. These features are the signature of a phase transition thwarted by the incommensurability of the lattice size with the periodicity of the order, inducing frustration. The phenomenon weakens when L increases, and could be handled using twisted boundary conditions.

Lastly, the energy distribution is unimodal for $J_3 < 0.6$, but becomes bimodal for system sizes of $L \geq 32$ (24) and $J_3 = 0.6$ (0.65), which is in favor of a first-order phase transition. For $J_3 = 0.67$, the energy distribution consists in two well separated peaks near T_c , even at low L and the phase transition is clearly first order.

For $0.69 \leq J_3 \leq 0.809$, Σ has large values in the low T phase and its susceptibility shows a peak which increases with L . For this reason, this transition will be discussed in the next paragraph, on the K_4 transition. Such K_4 transition is surprising here as the $T \rightarrow 0$ state is not supposed to break the K_4 symmetry: Σ should be zero in the non-octahedral ground state. Another phase transition thus seems unavoidable at lower T , restoring K_4 . In this hypothesis, the green dashed line of Fig. 9 was extended up to 0.809, implying a reentrance of the K_4 -breaking phase in the unconventional phase. The low- T phase transition would be first-order, as it relates phases with different broken symmetries. However, we did not succeed to evidence such a low- T phase transition, probably because of metastable states breaking K_4 , in which the simulations remains stucked despite the parallel tempering.

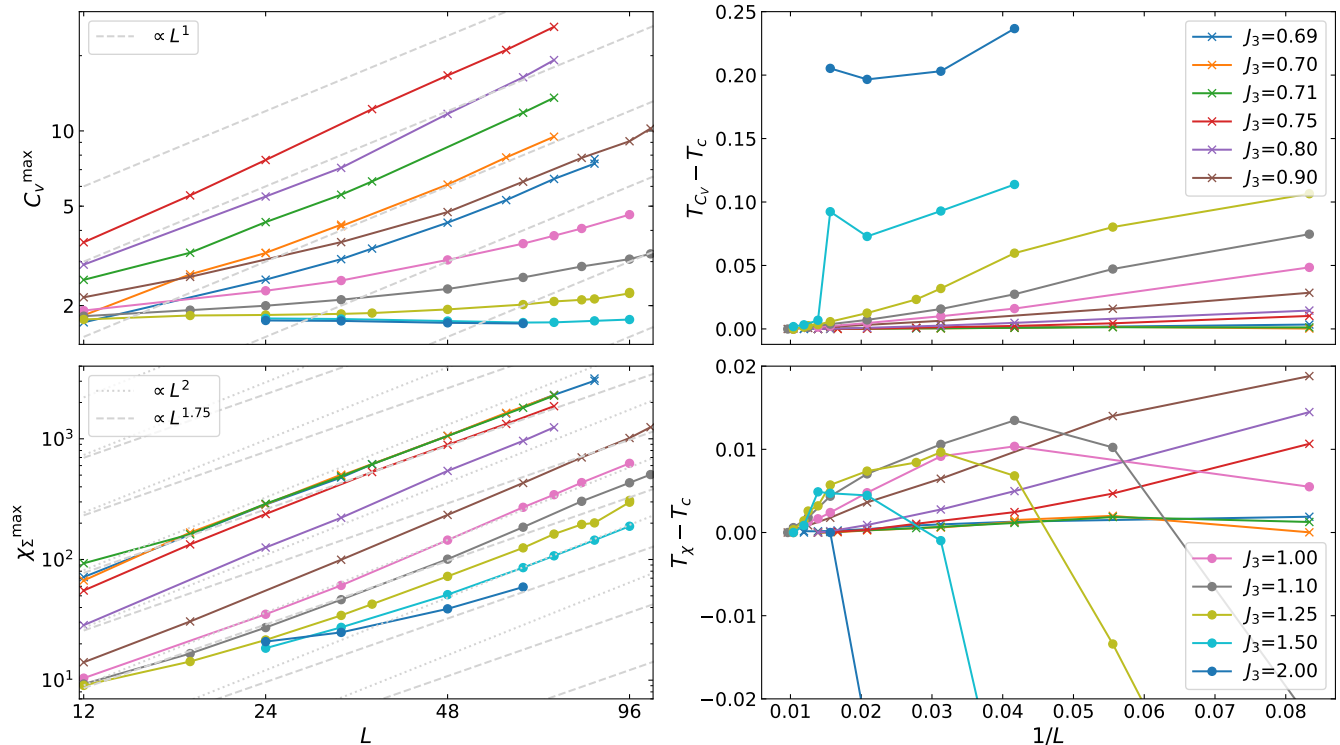


FIG. 10. Maximum of C_V and of χ versus the lattice size L for $J_1 = -1$ and various J_3 , and temperature of their maxima. T_c has been extracted from χ_Σ .

3. K_4 phase transition, in the unconventional and octahedral regions

For $J_3 \geq 0.69$, a transition occurs with both a C_V^{\max} and a χ_Σ^{\max} divergency with L , occuring at temperatures converging towards the same value $T_c(J_3)$. C_V^{\max} and of χ_Σ^{\max} have been collected for various of L and J_3 on Fig. 10, together with their temperatures. Finally, the Binder cumulant associated with Σ displays the behavior associated with a phase transition: it tends to $2/3$ below T_c when L increases and its curves for different L cross at the same temperature. This transition separates a low- T phase with large Σ from a nearly zero Σ high- T one. It corresponds to the restoration of the K_4 Potts symmetry, at a temperature $T_c(J_3)$ that increases with J_3 (Fig. 9). $T_c(J_3)$ is well fitted by $a(J_3 - J_3^c)^b$, with the three adjustable parameters $a = 0.88$, $b = 0.56$ and $J_3^c = 0.66$. We have here the proof that the order by disorder favors colinear states among the ground state manifold at low temperature.

Fig. 11 shows several quantities (Specific heat C_V , Potts magnetisation Σ , susceptibility χ and Binder parameter B) as a function of T for different system sizes, for $J_3 = 1$, as an illustration of a finite size scaling.

At low $J_3 \lesssim 1$, the energy distribution is weakly bimodal near T_c , which means that the two peaks are not well separated at low L . Both C_V and χ_Σ show a nice

divergency, at a temperature that extremely rapidly converges (Fig. 10), making the determination of the exponents related to it impossible due to precision issue. The exponents of the growth of χ_Σ is very near 2, which supports the hypothesis of a first order transition, but the one for C_V remains near 1, against 2 expected. It may be as a consequence of the unclear separation of the two peaks in the energy distribution, revealing a finite, but very large correlation length at the critical temperature, that would require simulations with larger lattice size. Another explanation would be that the transition becomes second ordered. Then, if it is in the universality class of the $q = 4$ Potts model, the exponents should be $\alpha/\nu = 1$ and $\gamma/\nu = 7/4$. These values are possible, but cannot be confirmed in view of our calculations.

The energy distribution at T_c becomes unimodal for $J_3 \gtrsim 1$ up to the explored lattice sizes. Together with this change, the maximum of the specific heat needs much larger lattice sizes to convincingly increase with L (Fig. 10). This is more and more pronounced when J_3 increases: for $J_3 \gtrsim 1.25$, we even see the appearance at large size of a secondary peak in C_V , that develops itself on the side of the main broad peak. For $J_3 = 1.5$, it only catches up the broad-peak maximum value at $L \simeq 64$, as can be seen on Fig. 10, where it translates in a dropout of T_{C_V} with L . It becomes tedious to extract critical exponents for C_V because the prefactor of the scaling

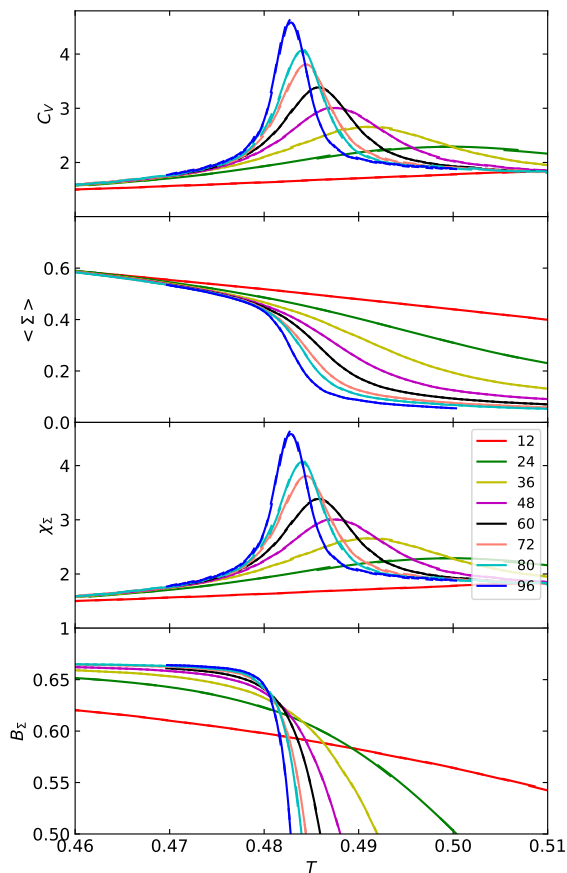


FIG. 11. Specific heat C_V , K_4 order parameter Σ , susceptibility χ_Σ and Binder parameter B_Σ versus T for different system sizes L for $J_1 = -1$ and $J_3 = 1$.

behavior is very small. The signature of the transition is still present in the scaling behavior of the order parameter: χ_Σ displays clear sign of divergency, even at small lattice sizes, with an exponent that remains near 2.

To conclude, we observe a phase transition for $J_3 > 0.69$ associated with Σ , that is weakly first order for small J_3 . With increasing J_3 , the first order transition still weakens, up to a point where it could be a second order transition. However, the critical exponents are difficult to determine due to the large sizes required to observe the leading order behavior of the maximum of C_V , but could correspond to those of the $q = 4$ Potts model. In the case of the antiferromagnetic $J_1 - J_2$ square lattice, where order by disorder tends to align spins for $J_2 > J_1/2$, the same difficulty was observed⁴⁹ when the sublattices become less coupled (when J_2 increases for the square lattice, J_3 for the kagomé).

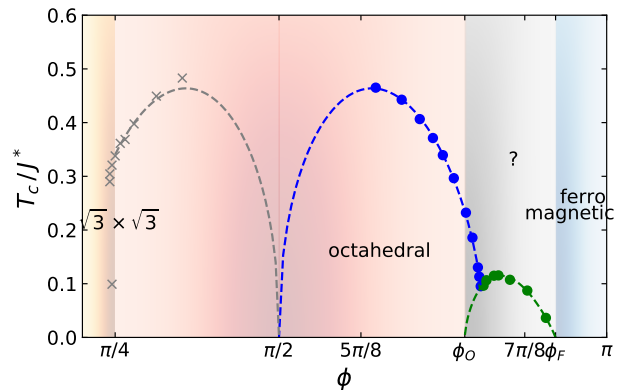


FIG. 12. Phase diagram of the $J_1 - J_3$ Heisenberg model on the kagomé lattice as a function of ϕ . Phase diagram obtained by Monte-Carlo simulation of the $J_1 - J_3$ model, in the $T - \phi$ plane. The blue and green points are those of Fig. 9, for $J_1 < 0$, with the same fits. Grey points are obtained for $J_1 > 0$, and the grey dashed line is obtained by symmetry of the blue one with respect to $\phi = \pi/2$.

C. Results for antiferromagnetic J_1

In order to explore the full octahedral phase of the phase diagram, we have also investigated the model with an antiferromagnetic interaction between the first nearest spins ($J_1 = 1$). However, this situation is not supposed to describe the Ba-Vesigneite compound. Simulation are performed for various positive values of J_3 and the transition temperatures are displayed on Fig. 12, which translates Fig. 9 in terms of ϕ and extends it to positive J_1 values. A astonishing similarity with the ferromagnetic J_1 is found: the transition temperature does not depend on the sign of J_1 for $J_3 > 1$, as emphasized on Fig. 12. It suggests that the critical temperature is only a function of $\sin \phi$ in a large neighborhood of $\phi = \pi/2$. Note that as soon as the leading term of $T_c(J_3)$ is weaker than $J_3/|J_1|$, $\lim_{\phi \rightarrow \pi/2} T_c(\phi) = 0$, which seems coherent as in this limit, the three sublattices are completely independent and no order is expected, at any temperature.

For $J_3 < 1$, the ground state is in the $\sqrt{3} \times \sqrt{3}$ phase and at low T , Σ is effectively very low. However, for $0.95 < J_3 < 1$, it sharply increases above a first critical temperature, and goes down again at a second one. This shows the existence of a reentrance of the K_4 symmetry broken phase in the $\sqrt{3} \times \sqrt{3}$ phase. This behavior is here more easily detected than in the unconventional phase, where it was only conjectured. This is probably due to the nature of the $\sqrt{3} \times \sqrt{3}$ low T phase, that here does not break any symmetry and must cause less thermalization issue.

V. QUANTUM AND THERMAL FLUCTUATIONS: LINEAR SPIN WAVE APPROXIMATION

An analytical approach to understand the emergence of a discrete order parameter, leading to a phase transition, consists in departing from one of the classical ground states, which are all equally favored at strictly zero temperature in the classical model, and to perturb it by adding infinitesimal thermal or quantum fluctuations (perturbing the classical state either by an infinitesimal T or $1/S$). We thus expect to lift the degeneracy between them. Thermal and quantum perturbations can be apprehended through the same formalism called the linear spin wave approximation. It will be developed in the two next subsections. But let us first develop the part which is common to both perturbations and define a set of eigenenergies $\omega_{\mathbf{q},l}$ which will be exploited differently in each case.

First, a reference ground state is chosen, whose spin orientation on site i is \mathbf{S}_i^0 . We then chose a rotation R_i such that $R_i \mathbf{S}_i^0 = \mathbf{e}_z$ and label by \mathbf{S}'_i the spin in the newly defined basis: $\mathbf{S}'_i = R_i \mathbf{S}_i$, whatever its orientation. \mathbf{S}'_i is either a real vector in the classical case, or an operator vector in the quantum case. In both cases, its norm is constrained by the spin length S . Using $S_i^{\prime\pm} = S'_{ix} \pm i S'_{iy}$, a vector \mathbf{U}_i is defined as:

$$\mathbf{U}_i = \begin{pmatrix} S_i^{\prime+} \\ S_i^{\prime-} \\ S_i^{\prime z} \end{pmatrix} = V \mathbf{S}'_i \quad V = \begin{pmatrix} 1 & i & 0 \\ 1 & -i & 0 \\ 0 & 0 & 1 \end{pmatrix} \quad (7)$$

The Hamiltonian written in terms of \mathbf{U}_i is:

$$H = \frac{1}{2} \sum_{i,j} \mathbf{U}_i \cdot \underbrace{(V R_i J_{i,j} R_j^{-1} V^{-1})}_{M_{i,j}} \mathbf{U}_j \quad (8)$$

We now expand the Hamiltonian with respect to a small parameter related to the distance of the actual state with the reference ground state: $S - S_i^{\prime z}$. We need here to focus successively on the low- T classical case and on the zero- T quantum case, to finally get the same eigenmodes in both situations.

To describe the quantum ground state, a Holstein-Primakoff transformation of the \mathbf{S}'_i spins is performed. It defines a_i^\dagger and a_i bosonic creation and annihilation operators on each site i . They are subject to a constraint on their number $n_i = a_i^\dagger a_i \leq 2S$, to respect the spin length. n_i is supposed to be $\mathcal{O}(1)$ in S :

$$\mathbf{U}_i = \begin{pmatrix} \sqrt{2S - a_i^\dagger a_i} \\ a_i^\dagger \sqrt{2S - a_i^\dagger a_i} \\ S - a_i^\dagger a_i \end{pmatrix} = \begin{pmatrix} \sqrt{2S} a_i + \mathcal{O}(S^{-1/2}) \\ \sqrt{2S} a_i^\dagger + \mathcal{O}(S^{-1/2}) \\ S - a_i^\dagger a_i \end{pmatrix} \quad (9)$$

The Hamiltonian now describes interacting bosons on the lattice.

On the classical side, by choosing as small complex parameter $z_i = \frac{S_i^{\prime+}}{\sqrt{2S}}$ and supposing it in $\mathcal{O}(1)$ (which is unjustified, as explained below), we get:

$$\mathbf{U}_i = \begin{pmatrix} \sqrt{2S} z_i \\ \sqrt{2S} z_i^* \\ \sqrt{S^2 - 2S|z_i|^2} \end{pmatrix} = \begin{pmatrix} \sqrt{2S} z_i \\ \sqrt{2S} z_i^* \\ S - |z_i|^2 + \mathcal{O}(S^{-1}) \end{pmatrix}. \quad (10)$$

The Hamiltonian (8) is now expanded in powers of $1/\sqrt{S}$. The first term is the energy of the reference classical ground state, in S^2 . The next term, in $S^{3/2}$, is zero if the reference ground state has correctly been chosen, as a stationary point of the reference energy with respect to the R_i 's. Finally, the first interesting term is in S , and has exactly the same form from Eq. (9) or from (10): it is a quadratic Hamiltonian either in a_i and a_i^\dagger or in z_i and z_i^* :

$$H^S = \frac{1}{2} \sum_{i,j} \mathbf{v}_i^\dagger M_{i,j}^S \mathbf{v}_j \quad (11)$$

where $M_{i,j}^S$ is a 2×2 matrix and \mathbf{v}_i is the two-component vector containing either a_i and a_i^\dagger or z_i and z_i^* .

Depending on the periodicity of $M_{i,j}^S$, an eventually large unit-cell of m sites is chosen to perform a Fourier transform $\tilde{\mathbf{v}}_{\mathbf{q}}$ of \mathbf{v}_i , of components:

$$\tilde{\mathbf{v}}_{\mathbf{q}} = \begin{pmatrix} \tilde{a}_{\mathbf{q},1} \\ \tilde{a}_{\mathbf{q},2} \\ \dots \\ \tilde{a}_{\mathbf{q},m} \\ (\tilde{a}_{-\mathbf{q},1})^\dagger \\ (\tilde{a}_{-\mathbf{q},2})^\dagger \\ \dots \\ (\tilde{a}_{-\mathbf{q},m})^\dagger \end{pmatrix}, \quad \begin{pmatrix} z_{\mathbf{q},1} \\ z_{\mathbf{q},2} \\ \dots \\ z_{\mathbf{q},m} \\ (z_{-\mathbf{q},1})^* \\ (z_{-\mathbf{q},2})^* \\ \dots \\ (z_{-\mathbf{q},m})^* \end{pmatrix}. \quad (12)$$

The Hamiltonian rewrites:

$$H^S = \frac{1}{2} \sum_{\mathbf{q}} (\tilde{\mathbf{v}}_{\mathbf{q}})^\dagger \cdot \tilde{M}_{\mathbf{q}}^S \tilde{\mathbf{v}}_{\mathbf{q}} + E_{\text{class}}, \quad (13)$$

where i and $j = 1 \dots m$ are now the indices of sites in the large unit cell and \mathbf{q} are wave vectors of a reduced Brillouin zone. The constant E_{class} results from commutation relations used in the quantum case, and has no effect in the classical expansion.

The eigenenergies $\omega_{\mathbf{q},l}$ are determined via a Bogoliubov transformation, that preserves the bosonic commutation relations in the quantum case, and the conjugation relations between z_i and z_i^* in the classical case. We thus define new vectors $\tilde{\mathbf{w}}_{\mathbf{q}}$ from a matrix $P_{\mathbf{q}}$ such that $P_{\mathbf{q}} \tilde{\mathbf{w}}_{\mathbf{q}} = \tilde{\mathbf{v}}_{\mathbf{q}}$, with properties similar to the $\tilde{\mathbf{v}}_{\mathbf{q}}$, that

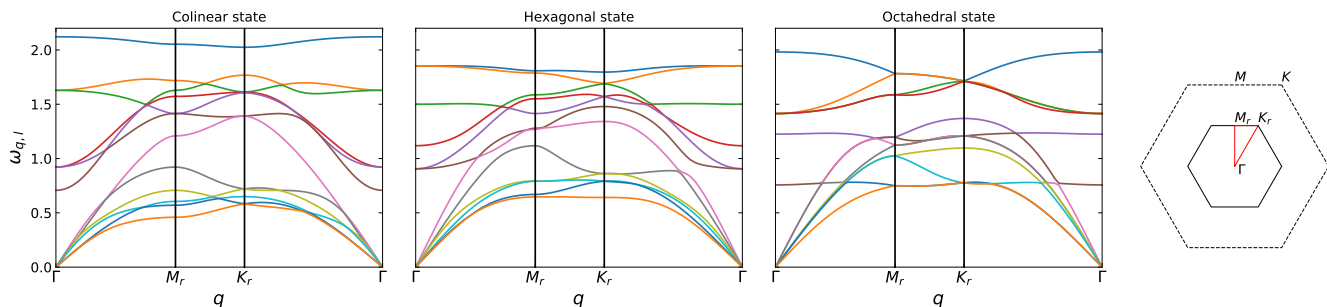


FIG. 13. Dispersion relations $\omega_{\mathbf{q},l}$ along a cut in the Brillouin zone (red line on the right) from linear spin wave approximation for $\phi = 3\pi/4$ ($J_3 = -J_1 > 0$) for the $J_1 - J_3$ kagomé model, for the three ground states of Fig. 3. As a unit cell of 12 sites has been chosen, there are 12 energy bands in the reduced Brillouin zone (full black line on the right).

are eigenmodes of the Hamiltonian (the transformed $\tilde{M}_{\mathbf{q}}^S$ matrix is diagonal). The information that we can extract from $P_{\mathbf{q}}$ and $\omega_{\mathbf{q},l}$ in the quantum and classical cases will be described in the next subsections.

We now apply this formalism to the $J_1 - J_3$ model, in the octahedral part of the phase diagram (Fig. 2). A generic ground state is chosen, parametrized by three angles θ_B , θ_C and ϕ_C where spins in the origin unit cell (on the green, blue and red sites of the marron triangle of Fig. 4) are:

$$\mathbf{S}_A^0 = \begin{pmatrix} 0 \\ 0 \\ 1 \end{pmatrix}, \mathbf{S}_B^0 = \begin{pmatrix} \sin \theta_B \\ 0 \\ \cos \theta_B \end{pmatrix}, \mathbf{S}_C^0 = \begin{pmatrix} \sin \theta_C \cos \phi_C \\ \sin \theta_C \sin \phi_C \\ \cos \theta_C \end{pmatrix}. \quad (14)$$

This parametrization describes all the ground states, up to a global spin rotation (equivalent to an appropriate choice of the basis in the spin space). Moreover, up to a lattice translation, we can fix $0 \leq \theta_B, \theta_C \leq \pi/2$, $0 \leq \phi_C \leq \pi$. The three states of the bottom of Fig. 3 are given from left to right by $(\theta_B, \theta_C, \phi_C) = (0, 0, 0)$ (colinear state), $(\pi/3, \pi/3, \pi)$ (hexagonal) and $(\pi/2, \pi/2, \pi/2)$ (octahedral).

To perform the Fourier transformation of Eq. (13), a unit-cell of 12 sites has to be chosen (as on Fig. 6), which results in 24×24 $\tilde{M}_{\mathbf{q}}^S$ matrices. The dispersion relations for $\phi = 3\pi/4$ ($J_3 = -J_1 > 0$) are given in Fig. 13 for the colinear, hexagonal and octahedral states.

A. Linear thermal spin wave approximation

In two dimensions, we cannot expect to have a valid expansion at finite temperature: the Mermin-Wagner theorem predicts that a continuous order parameter (here the spin orientation), cannot survive to infinitesimal temperature. The hypothesis done on the small fluctuations around the classical ground state is false. However, short range correlations survive, and their nature can still be inferred from entropic selection of the maximally fluctuating ground state at low temperatures^{38,50}.

Classical spins are described, in the linear spin wave approximation, by a collection of independent harmonic oscillators of frequencies $\omega_{\mathbf{q},l}$. There are two modes for each couple (\mathbf{q}, l) , associated with the real (x spin component) and imaginary (y spin component) part of z_i in Eq. (10). At finite temperature, the free energy $F = E - TS$ depends on the reference ground state which has been chosen. E is the same for all of them, thus, it is the entropy that lifts the degeneracy. For a classical harmonic oscillator of frequency ω , the entropy is $S = \text{const} - \ln \frac{T}{\omega}$. A zero point energy is necessary to forbid negative values of the entropy at low temperature. The entropies of different reference ground states are parametrized by the angles $S(\theta_B, \theta_C, \phi_C)$ of Eq. (14), or more conveniently, by the vector of spin dot-products $\boldsymbol{\sigma}$, defined in Sec. III B. The difference $\Delta S(\theta_B, \theta_C, \phi_C) = S(\theta_B, \theta_C, \phi_C) - S(0, 0, 0)$, or equivalently $\Delta S(\boldsymbol{\sigma}) = S(\boldsymbol{\sigma}) - S(\boldsymbol{\sigma}_0)$, where $\boldsymbol{\sigma}_0 = (1, 1, 1)$, does not depend on the temperature and is represented on Fig. 14 for $\phi = 3\pi/4$. The maximum is reached in the colinear state, and the minimum in the octahedral state, as expected.

B. Linear quantum spin wave approximation

In quantum materials, the spin has a finite value ($S = 1/2, 1, 3/2, \dots$), which differs from the classical case corresponding to the limit $S \rightarrow \infty$. In Ba-Vesignieite, the spin on the copper sites has the most quantum value of $1/2$. We now discuss the consequences in light of the previous classical considerations. Quantum fluctuations tend to disorder the system: a model with a magnetically ordered ground state in the classical limit generally has an order parameter m that decreases when S decreases. We thus face two possibilities: either the order parameter remains finite ($m > 0$) when quantum fluctuations are switched on, or it reaches zero and the ground state is no more long-range ordered.

The linear spin wave approximation expands to first non trivial order quantum observables (as the energy or an order parameter) in $1/\sqrt{S}$ at zero temperature and

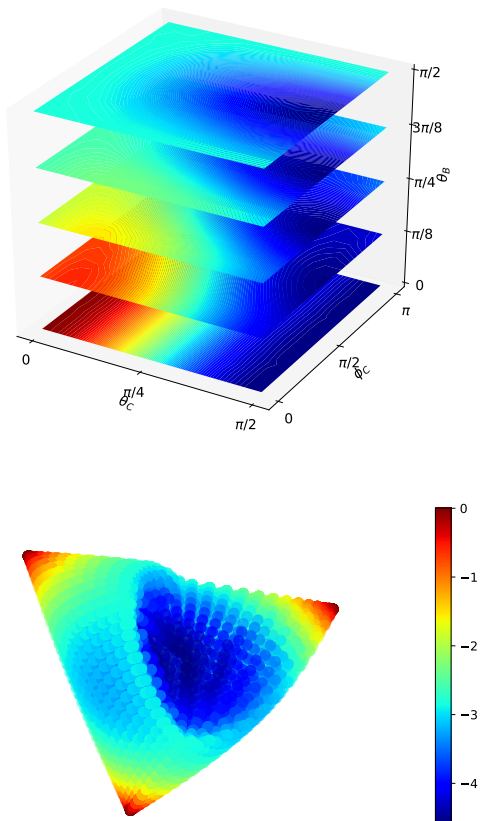


FIG. 14. Low energy entropy $\Delta S(\theta_B, \theta_C, \phi_C)$ (top) and $\Delta S(\sigma)$ (bottom), where the angles were defined in Eq. (14) and σ in Sec. III B, for $J_1 < 0$ and $J_3 = -J_1$. The maximal entropy (in dark red) is for $\theta_B = \theta_C = 0$: the colinear state, and the minimum (in dark blue) for $\theta_B = \theta_C = \phi_C = \pi/2$: the octahedral state, corresponding respectively to the vertices and to the center of the inflated tetrahedron formed by the set of σ values.

around a specific ground state. When several ground states exist, as occurs here in the $J_1 - J_3$ model, the expansion can be performed around any of them, giving different correction to the energy that eventually lifts the degeneracy. The first terms of the energy are:

$$E = S(S+1)E_{\text{class}} - \frac{S}{2} \sum_{\mathbf{q}, l} \omega_{\mathbf{q}, l} + \mathcal{O}(\sqrt{S}), \quad (15)$$

where $E_{\text{class}} = -2J_3$ in the octahedral phase. The term of order S : $\Delta E = E_{\text{class}} - \frac{1}{2} \sum_{\mathbf{q}, l} \omega_{\mathbf{q}, l}$, depends on the angles $(\theta_B, \theta_C, \phi_C)$ and on the coupling ϕ . It can be represented in the same way as ΔS in Fig. 14 for a fixed ϕ . The same qualitative behavior is obtained, and the same conclusion: the colinear state is the most favored by quantum fluctuations, whereas the octahedral one has the weakest quantum energy correction. It is quite expected that quantum and thermal fluctuations favor the

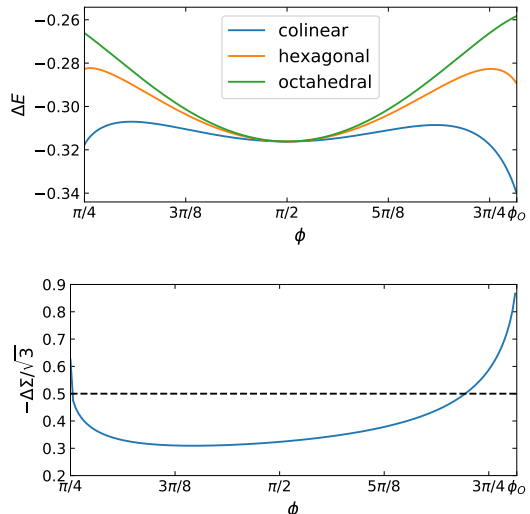


FIG. 15. Results of quantum linear spin wave approximation for $(J_1, J_3) = (\cos \phi, \sin \phi)$, in the octahedral phase of Fig. 2. Top: correction ΔE of order S to the energy around the three classical states depicted in Fig. 3. Bottom: correction $\Delta \Sigma$ of order S to the order parameter for the colinear phase. The dashed line indicates an approximative value of $-\Delta \Sigma / \sqrt{3}$ above which quantum fluctuations restore the K_4 symmetry for $S = 1/2$.

same order, even if counter-examples exist⁵¹. For completeness, the curve of ΔE is given versus ϕ in Fig. 15, for the three ground states of Fig. 3. Whatever ϕ (except $\phi = \pi/2$ where the three sublattices are completely decoupled), quantum fluctuations always favor the colinear state.

The order parameter Σ can be expanded as the energy: $\Sigma = S^2 \Sigma_{\text{class}} + S \Delta \Sigma + \mathcal{O}(\sqrt{S})$, which can be used as an indication of the critical spin where its average cancels, excluding the occurrence of a phase transition as finite temperature. The classical value is $\Sigma_{\text{class}} = \sqrt{3}$. Thus, $S_c \sim -\frac{\Delta \Sigma}{\sqrt{3}}$. S_c is below 1/2 in all the octahedral phase, except near the boundary with the unconventional phase (Fig. 15). It suggesting that the K_4 symmetry could be broken even in the $S = 1/2$ case.

VI. HIGH TEMPERATURE SERIES EXPANSIONS (HTSE)

After a look at the behavior of the model from the classical limit ($S = \infty$) towards finite spins, the extreme quantum case of $S = 1/2$ can be investigated through high temperature series expansions. The logarithm of the partition function $\frac{\ln Z}{N}(\beta)$ is expanded in powers of the inverse temperature β directly in the thermodynamic

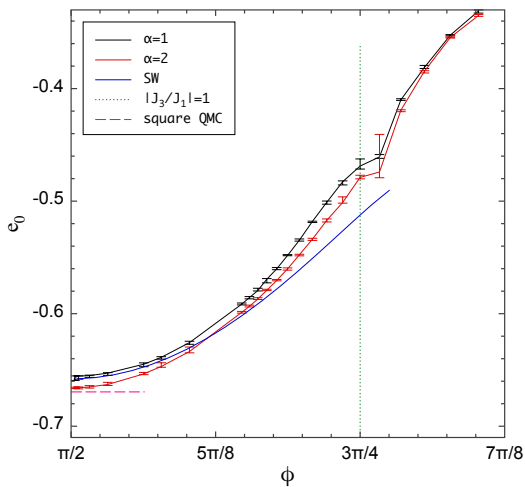


FIG. 16. Ground state energy per site e_0 as a function of ϕ , with $(J_1, J_3) = (\cos \phi, \sin \phi)$ on the kagomé lattice. e_0 is obtained via the method described in Bernu *et al.*⁵², using high temperature series expansions up to order 15. The red and black points are the results with the hypothesis that $C_V \sim AT^\alpha$, with $\alpha = 1$ and 2 and A a constant. The blue curve is the linear spin wave energy up to order S , approximated for $S = 1/2$.

limit:

$$\lim_{N \rightarrow \infty} \frac{\ln Z}{N}(\beta) = \ln 2 + \sum_{n=1}^{\infty} \left(\sum_{i=0}^n Q_{i,n} J_1^i J_3^{n-i} \right) \beta^n, \quad (16)$$

where N is the number of lattice sites. Enumerating connected clusters on the $J_1 - J_3$ kagomé lattice, we exactly calculate the coefficients of this series up to order 15 in β , each of them being an homogeneous polynomial in J_1 and J_3 .

A direct use of the truncated series to evaluate thermodynamical functions is doomed to fail, as the series only converges for $T \gtrsim J_1, J_3$. An extrapolation technique called the entropy method (HTSE+ $s(e)$) has been developed^{53,54}, that extrapolates functions from infinite down to zero temperatures. It uses the hypothesis of the absence of finite temperature phase transition, so that the functions are analytical over the full temperature interval. It also requires some inputs: the ground state energy per site e_0 and the low temperature behavior of C_V (in power law $C_V \sim T^\alpha$, or exponential for example), what can be understood as the need to constrain the thermodynamical functions both from the $T = \infty$ side, which is ensured by the series coefficients, and from the $T = 0$ one.

The need for e_0 is a real problem, as no generic method exist to determine it in the case of frustrated quantum models. In Bernu *et al.*⁵², a self-consistent method has been developed that proposes an e_0 . Although no rigorous argument says that this energy is near the real one, it has been shown to give extremely coherent results

on the first neighbor kagome model. With the hypothesis that no phase transition occurs, the ground state energy e_0 obtained by this method is shown in Fig. 16, for $C_V \sim_{T \rightarrow 0} AT^\alpha$ with $\alpha = 2$ (which is the case for $\phi = \pi/2$) and $\alpha = 1$. The minimal $\phi = \pi/2$ on Fig. 16 corresponds to the three decoupled square sub-lattices, whose ground state energy is accessible through quantum Monte Carlo simulations in this unfrustrated case: $e_0 = -0.6695$ ^{55,56}. HTSE+ $s(e)$ results give still better results than the linear spin wave approximation. With increasing ϕ , error bars increase and the result quality becomes bad in the neighborhood of ϕ_O (convergence issue of the method), at the point where a slope breaking occurs in $e_0(\phi)$.

In view of the previous sections, this behavior can be attributed to the existence of a phase transition at finite temperature T_c near ϕ_O . In the Supp. Mat. of⁵⁴, the possibility to detect a phase transition thanks to HTSE+ $s(e)$ was proposed for a ferromagnetic BCC lattice, where e_0 was exactly known and the extrapolation was performed down to $T = 0$ despite the singularity at T_c . Here, the method tends to deviate e_0 from its real value to get rid of eventual singularities. We propose a new adaptation of HTSE+ $s(e)$ to models with phase transitions, that will be detailed elsewhere⁵⁷. The extrapolation is only done on the temperature interval $[T_c, \infty]$, requiring as supplementary input parameters T_c , the energy e_c and the entropy s_c at T_c . We also characterize the behavior of C_V near the transition by an exponent α :

$$C_V(T) \sim_{T \rightarrow T_c^+} \frac{A}{(T - T_c)^\alpha}. \quad (17)$$

Because of the sum rules on $C_V(T)/T$, α must be lower or equal to 1. For $J_1 = -1$ and $J_3 = 1$, the four parameters T_c , e_c , s_c and α giving the higher quality of result were looked for. Interesting values are found in a tiny valley of the 4 dimensional space, with a transition at $T_c = 0.42(1)$ and an exponent of $\alpha = 0.29(1)$, $e_c = -0.405(5)$ and $s_c = 0.35(1)$.

Even if still exploratory, this section on HTSE confirm the possibility of a phase transition in the $S = 1/2$ model, in the domain of parameter where it is the more easily detected in the classical model: $J_3 \simeq |J_1|$.

VII. CONCLUSION

Motivated by the Ba-Vesignieite compound, this article has explored the $J_1 - J_3$ model on the kagomé lattice, in the domain of large J_3 . The classical phase diagram has revealed interesting phases: for ferromagnetic J_1 and moderate J_3 , an unconventional phase displays conical, spiral, and probably other unusual phases, whereas for large J_3 , whatever the sign of J_1 , an octahedral phase possesses an accidental degeneracy. Thermal or quantum fluctuations lift this degeneracy via the order by disorder mechanism, favouring collinear configurations, labelled by

an element of the K_4 group. An order parameter Σ was constructed by analysing the symmetries of the model, to detect this discrete K_4 symmetry breaking.

Classical Monte Carlo simulations have evidenced an order-by-disorder induced phase transition associated with Σ . The transition is first order for low J_3 's, and either weakly first order or second order for large ones. Other phase transitions were found in the unconventional phase, associated with one or several other order parameters.

Linear spin wave formalism have shown that both thermal and quantum fluctuations favor the colinear states. But quantum fluctuations can be so strong that they completely disorder the system, preventing the occurrence of a phase transition, notably near the boundary with the unconventional phase $\phi = \phi_O$. Finally, HTSEs also confirm the possibility of a phase transition, this time in the $S = 1/2$ model.

What are the implication of this phase transition on Ba-Vesignieite ? First of all, the dominant coupling was proposed to be J_3 in¹², but the one coming next was J'_3 , then J_1 , and J_2 . We did not considered J'_3 as it did not couple the three kagomé sublattices, and have focused on J_1 . Note that J_2 would have led to the same order by disorder effect as J_1 . One could argue that many perturbations other than next nearest neighbor interactions can lift the degeneracy of the octahedral phase. Among them, a slight distortion of the lattice is known, of less than 1% of the Cu-Cu distance and causes a coupling anisotropy¹³. Some impurities are unavoidable, whose effect has been studied on the $J_1 - J_2$ square lattice. Their effect is opposite to the one of thermal fluctuation, selecting orthogonal configurations^{38,50}, and penalizing colinear ones. If this occurs here, the octahedral state of Fig. 3 would be favored, possibly leading to a chiral phase transition. Dzyaloshinskii-Moriya interactions must also be present⁵⁸, as well as Ising spin anisotropy¹² but eventually very small. Lastly, a small coupling between spins in successive kagomé planes exists and is suspected to induce the phase transition observed at $T = 9K$ ¹².

However, despite this whole set of deviations from the $J_1 - J_3$ model, the transition discussed in this article remains meaningful. At temperature larger than their typical value, their effect is crushed, and the K_4 order can still be present.

Lastly, the theoretical investigation of such an emerging $q = 4$ Potts order parameter and of its phase transition illustrate in an original way the order by disorder mechanism.

ACKNOWLEDGMENTS

We thank Bjorn Fåk for discussions on the experimental results on Vesignieite. This work was supported by the French Agence Nationale de la Recherche under Grants No. ANR-18-CE30-0022-04 LINK.

Numerical simulations were performed on the highly

parallel computer of the LJP, LKB and LPTMC.

Appendix A: The Luttinger-Tizsa method

To use the LT method, we perform a Fourier transform on H . With this in mind, we rewrite Eq. (1)

$$H = \frac{1}{2} \sum_{\mathbf{r}} \sum_{\mathbf{v}} \sum_{i,j} J_{i,j}(\mathbf{v}) \mathbf{S}_{i,\mathbf{r}} \cdot \mathbf{S}_{j,\mathbf{r}+\mathbf{v}}, \quad (\text{A1})$$

where $\mathbf{r}, \mathbf{r} + \mathbf{v}$ are vectors from a Bravais lattice locating the unit-cells of the interacting spins, i and j label inequivalent sites in each unit-cell. Next, we introduce the Fourier modes of a spin i in cell \mathbf{r} :

$$\mathbf{S}_{i,\mathbf{r}} = \frac{1}{\sqrt{N}} \sum_{\mathbf{q}} \tilde{\mathbf{S}}_i(\mathbf{q}) e^{i\mathbf{q}\cdot\mathbf{r}}, \quad (\text{A2})$$

to rewrite the Hamiltonian as:

$$H = \frac{1}{2} \sum_{\mathbf{q}} \sum_{i,j} \tilde{\mathbf{S}}_i(\mathbf{q}) \tilde{J}_{i,j}(\mathbf{q}) \tilde{\mathbf{S}}_j(-\mathbf{q}) \quad (\text{A3})$$

where $\tilde{J}_{i,j}(\mathbf{q}) = \sum_{\mathbf{v}} J_{i,j}(\mathbf{v}) e^{i\mathbf{q}\cdot\mathbf{v}}$ is akin to a Fourier transform of the couplings of H . The Hamiltonian itself is now expressed as a bilinear form in the Fourier modes $\tilde{\mathbf{S}}_i(\mathbf{q})$. Its ground state may easily be found by diagonalizing $\tilde{J}(\mathbf{q})$ and minimizing its lowest eigenvalue $\lambda_{\min}(\mathbf{q})$ with respect to \mathbf{q} . This, in turn, leads us to a generally discrete set of wave vectors \mathbf{q}_i of the Brillouin zone respecting the lattice symmetries⁵⁹. The desired ground state is then obtained by solely populating the eigenmodes corresponding to $\lambda_{\min}(\mathbf{q}_i)$ and performing an inverse Fourier transform.

In the preceding paragraph we never mentioned the nature of the lattice - Bravais or not - in order to justify the steps we took. One can wonder why, then, is it not possible to apply the LT methodology to our particular instance of the problem. The answer lies in an unmentioned constraint we ought to abide by: at each site we have a unit spin \mathbf{S}_i , with $\|\mathbf{S}_i\| = 1$. For Bravais lattices this is not an issue, since there always exists a spiral state, defined by a single wavevector, which is a ground state of the Hamiltonian. For non-Bravais lattices, however, such as the kagomé lattice we're working on, this constraint prevents us from applying the last step, as naively populating a mode with the lowest energy generally does not respect the constraint on all sites of a unit cell. Thus, other modes can be used to recover the constraint, increasing the energy as compared with λ_{\min} , which is then only a lower bound.

Appendix B: Summary of results on the Potts model

The critical exponents of the two-dimensional Potts mode have a conjectured exact expression for $q \leq 4$

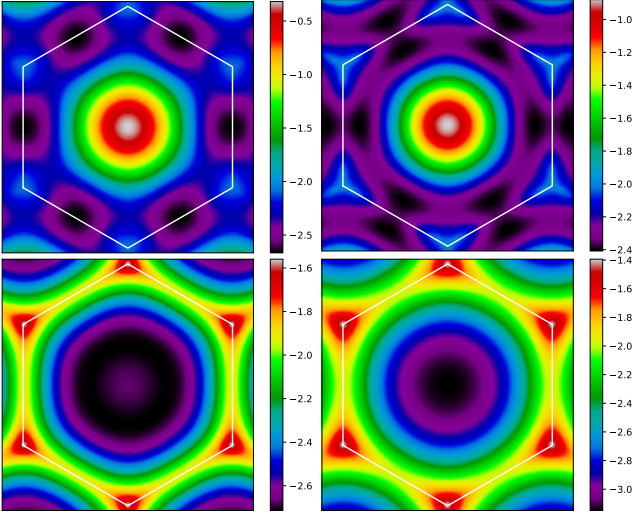


FIG. 17. $\lambda_{\min}(\mathbf{q})$ for the $J_1 - J_3$ model on the kagomé lattice with $\phi = \phi_O - 0.05$ (top left), $\phi_O + 0.05$ (top right) $\phi = \phi_F - 0.05$ (bottom left), $\phi_F + 0.05$ (bottom right).

(See⁴⁶), that leads to:

$$\alpha = \frac{2}{3}, \quad \gamma = \frac{7}{6}, \quad \beta = \frac{1}{12},$$

$$\delta = 15, \quad \nu = \frac{2}{3}, \quad \eta = \frac{1}{4}$$

Appendix C: Determination of the value of ϕ_O

We present here a derivation of the value of ϕ_O , where the transition between the orthogonal and unconventional phase occurs in the $J_1 - J_3$ model on the kagomé lattice (see Fig. 2). The proof rests on the LT method presented in App. A. The $\tilde{J}(\mathbf{q})$ matrix of Eq. (A3), multiplied by the overall $\frac{1}{2}$, writes:

$$\begin{pmatrix} J_3(c_1^2 + c_2^2 - 1) & \frac{J_1}{2}c_1 & \frac{J_1}{2}c_2 \\ \frac{J_1}{2}c_1 & J_3(c_1^2 + c_3^2 - 1) & \frac{J_1}{2}c_3 \\ \frac{J_1}{2}c_2 & \frac{J_1}{2}c_3 & J_3(c_2^2 + c_3^2 - 1) \end{pmatrix}, \quad (\text{C1})$$

where $c_1 = \cos \frac{q_x}{2}$, $c_2 = \cos \frac{q_y}{2}$ and $c_3 = \cos \frac{q_x - q_y}{2}$.

In the octahedral phase, the minimal eigenvalue $\lambda_{\min}(\mathbf{q})$ of $\tilde{J}(\mathbf{q})$ occurs for three \mathbf{q} : $\mathbf{M}_{1,2,3}$, the middles of the edges of the Brillouin zone (see Fig.17). At the transition toward the unconventional phase, each of the

three minima splits in two, giving six new minima evolving with ϕ along the line $M_i - \Gamma$.

The characteristic polynomial $C(\lambda)$ of the $\tilde{J}_{i,j}(\mathbf{M}_1 + \delta\mathbf{q})$ matrix is expanded to the first order in $\epsilon = \lambda + 2J_3$, as we look for the minimal root of $C(\lambda)$, which is nearby $-2J_3$ (the energy of an octahedral state) in the neighborhood of $\mathbf{M}_1 = (\pi, 0)$ and for the values of J_3 and J_1 of interest. The root of the first order degree polynomial approximating $C(\lambda)$ is expanded to the second order in $\delta\mathbf{q}$. Increasing from $\phi = \pi/2$, the quadratic form thus obtained changes at $\phi = \phi_t = \pi - \arctan \frac{1+\sqrt{5}}{4}$ from a positive one, with a minima at $\delta\mathbf{q} = \mathbf{0}$, to a non-positive one, with a saddle point at $\delta\mathbf{q} = \mathbf{0}$, indicating that the energy of the octahedral state is no more the lower bound, and that $\phi_O \geq \phi_t$ (they are unequal if the octahedral phase remains the ground state in the area where it does not have the LT lower bound energy).

It remains to exhibit a state that has a lower energy than the octahedral state for $\phi > \phi_t$ to prove that ϕ_t is effectively the transition value. This is done using the conical state of Fig. 5. We parametrize it by four angles (θ, ϕ, ψ) . A unit cell of 12 sites is defined as indicated on Fig. 5, with three different spin orientations $\mathbf{S}_{1,2,3}$. A translation in the \mathbf{e}_1 direction has no effect on the spin orientation, whereas a translation in the \mathbf{e}_2 (y coordinate) rotates the spins of ϕ and inverse them:

$$\mathbf{S}_1 = (-1)^y \begin{pmatrix} \cos 2y\psi \\ \sin 2y\psi \\ 0 \end{pmatrix},$$

$$\mathbf{S}_2 = (-1)^y \begin{pmatrix} -\sin \phi \sin((2y-1)\psi) \\ \sin \phi \cos((2y-1)\psi) \\ \cos \phi \end{pmatrix},$$

$$\mathbf{S}_3 = (-1)^y \begin{pmatrix} -\sin \phi \sin((2y-1)\psi) \\ \sin \phi \cos((2y-1)\psi) \\ -\cos \phi \end{pmatrix} \quad (\text{C2})$$

The energy per site thus reads:

$$E = \frac{2J_1 \sin \phi}{3} (\sin \psi (1 - \cos 2\psi) - \cos \psi \sin 2\psi + \sin \phi) + \frac{2J_3}{3} (2 \sin^2 \phi \sin^2 \psi - \cos 2\psi - 2 \cos^2 \phi)$$

The minimum of this energy (numerically obtained) is effectively between the lowest bound and the energy of the octahedral state for $\phi \gtrsim \phi_O$ (see the inset of Fig. 2, bottom)

* viot@lptmc.jussieu.fr
† bernu@lptmc.jussieu.fr
‡ messio@lptmc.jussieu.fr

¹ L. Savary and L. Balents, Quantum spin liquids: a review, Reports on Progress in Physics **80**, 016502 (2017).
² M. A. de Vries, J. R. Stewart, P. P. Deen, J. O. Piatek,

- G. J. Nilsen, H. M. Rønnow, and A. Harrison, Scale-free antiferromagnetic fluctuations in the $s = 1/2$ kagome antiferromagnet herbertsmithite, *Phys. Rev. Lett.* **103**, 237201 (2009).
- ³ B. Fåk, E. Kermarrec, L. Messio, B. Bernu, C. Lhuillier, F. Bert, P. Mendels, B. Koteswararao, F. Bouquet, J. Ollivier, A. D. Hillier, A. Amato, R. H. Colman, and A. S. Wills, Kapellasite: A Kagome Quantum Spin Liquid with Competing Interactions, *Phys. Rev. Lett.* **109**, 037208 (2012).
 - ⁴ Z. Hiroi, H. Yoshida, Y. Okamoto, and M. Takigawa, Spin-1/2 kagome compounds: Volborthite vs Herbertsmithite, *J. Phys.: Conf. Ser.* **145**, 012002 (2009).
 - ⁵ R. Colman, A. Sinclair, and A. Wills, Comparisons between haydeite, α - $\text{Cu}_3\text{Mg}(\text{OH})_6\text{Cl}_2$, and kapellasite, α - $\text{Cu}_3\text{Zn}(\text{OH})_6\text{Cl}_2$, isostructural $s = 1/2$ kagome magnets, *Chem. Mater.* **22**, 5774 (2010), <http://pubs.acs.org/doi/pdf/10.1021/cm101594c>.
 - ⁶ R. H. Colman, A. Sinclair, and A. S. Wills, Magnetic and crystallographic studies of mg-herbertsmithite, γ - $\text{Cu}_3\text{Mg}(\text{OH})_6\text{Cl}_2$ a new $s = 1/2$ kagome magnet and candidate spin liquid, *Chemistry of Materials* **23**, 1811 (2011), <https://doi.org/10.1021/cm103160q>.
 - ⁷ Y. Okamoto, H. Yoshida, and Z. Hiroi, Vesignieite $\text{BaCu}_3\text{V}_2\text{O}_8(\text{OH})_2$ as a Candidate Spin-1/2 Kagome Antiferromagnet, *Journal of the Physical Society of Japan* **78**, 033701 (2009).
 - ⁸ H. Yoshida, Y. Michiue, E. Takayama-Muromachi, and M. Isobe, Vesignieite $\text{BaCu}_3\text{V}_2\text{O}_8(\text{OH})_2$: a structurally perfect $S = 1/2$ kagomé antiferromagnet, *J. Mater. Chem.* **22**, 18793 (2012).
 - ⁹ Y. Okamoto, M. Tokunaga, H. Yoshida, A. Matsuo, K. Kindo, and Z. Hiroi, Magnetization plateaus of the spin-1/2 kagome antiferromagnets volborthite and vesignieite, *Phys. Rev. B* **83**, 180407 (2011).
 - ¹⁰ H. Ishikawa, T. Yajima, A. Miyake, M. Tokunaga, A. Matsuo, K. Kindo, and Z. Hiroi, Topochemical Crystal Transformation from a Distorted to a Nearly Perfect Kagome Cuprate, *Chemistry of Materials* **29**, 6719 (2017), <https://doi.org/10.1021/acs.chemmater.7b01448>.
 - ¹¹ A. Verrier, F. Bert, J. M. Parent, M. El-Amine, J. C. Orain, D. Boldrin, A. S. Wills, P. Mendels, and J. A. Quilliam, Canted antiferromagnetic order in the kagome material Sr-vesignieite, *Phys. Rev. B* **101**, 054425 (2020).
 - ¹² D. Boldrin, B. Fåk, E. Canévet, J. Ollivier, H. C. Walker, P. Manuel, D. D. Khalyavin, and A. S. Wills, Vesignieite: An $S = \frac{1}{2}$ Kagome Antiferromagnet with Dominant Third-Neighbor Exchange, *Phys. Rev. Lett.* **121**, 107203 (2018).
 - ¹³ R. H. Colman, F. Bert, D. Boldrin, A. D. Hillier, P. Manuel, P. Mendels, and A. S. Wills, Spin dynamics in the $S = \frac{1}{2}$ quantum kagome compound vesignieite, $\text{Cu}_3\text{Ba}(\text{VO}_5\text{H})_2$, *Phys. Rev. B* **83**, 180416 (2011).
 - ¹⁴ J. A. Quilliam, F. Bert, R. H. Colman, D. Boldrin, A. S. Wills, and P. Mendels, Ground state and intrinsic susceptibility of the kagome antiferromagnet vesignieite as seen by ^{51}V NMR, *Phys. Rev. B* **84**, 180401 (2011).
 - ¹⁵ J.-C. Dornenge, P. Sindzingre, C. Lhuillier, and L. Pierre, Twelve sublattice ordered phase in the $J_1 - J_2$ model on the kagomé lattice, *Phys. Rev. B* **72**, 024433 (2005).
 - ¹⁶ L. Messio, B. Bernu, and C. Lhuillier, Kagome Antiferromagnet: A Chiral Topological Spin Liquid?, *Phys. Rev. Lett.* **108**, 207204 (2012).
 - ¹⁷ L. Messio, C. Lhuillier, and G. Misguich, Lattice symmetries and regular magnetic orders in classical frustrated antiferromagnets, *Phys. Rev. B* **83**, 184401 (2011).
 - ¹⁸ S. R. Sklan and C. L. Henley, Nonplanar ground states of frustrated antiferromagnets on an octahedral lattice, *Phys. Rev. B* **88**, 024407 (2013).
 - ¹⁹ N. D. Mermin and H. Wagner, Absence of Ferromagnetism or Antiferromagnetism in One- or Two-Dimensional Isotropic Heisenberg Models, *Phys. Rev. Lett.* **17**, 1133 (1966).
 - ²⁰ N. D. Mermin, Absence of ordering in certain classical systems, *Journal of Mathematical Physics* **8**, 1061 (1967), <https://doi.org/10.1063/1.1705316>.
 - ²¹ A. Klein, L. J. Landau, and D. S. Shucker, On the absence of spontaneous breakdown of continuous symmetry for equilibrium states in two dimensions, *Journal of Statistical Physics* **26**, 505 (1981), <https://doi.org/10.1007/BF01011431>.
 - ²² J. M. Kosterlitz and D. J. Thouless, Ordering, metastability and phase transitions in two-dimensional systems, *Journal of Physics C: Solid State Physics* **6**, 1181 (1973).
 - ²³ H. W. J. Blöte, W. Guo, and H. J. Hilhorst, Phase Transition in a Two-Dimensional Heisenberg Model, *Phys. Rev. Lett.* **88**, 047203 (2002).
 - ²⁴ M. E. Zhitomirsky and K. Ueda, Valence-bond crystal phase of a frustrated spin-1/2 square-lattice antiferromagnet, *Phys. Rev. B* **54**, 9007 (1996).
 - ²⁵ J.-C. Dornenge, C. Lhuillier, L. Messio, L. Pierre, and P. Viot, Chirality and \mathbb{Z}_2 vortices in a Heisenberg spin model on the kagome lattice, *Phys. Rev. B* **77**, 172413 (2008).
 - ²⁶ L. Messio, J.-C. Dornenge, C. Lhuillier, L. Pierre, P. Viot, and G. Misguich, Thermal destruction of chiral order in a two-dimensional model of coupled trihedra, *Phys. Rev. B* **78**, 054435 (2008).
 - ²⁷ T. A. Kaplan and N. Menyuk, Spin ordering in three-dimensional crystals with strong competing exchange interactions, *Philosophical Magazine* **87**, 3711 (2007), <https://doi.org/10.1080/14786430601080229>.
 - ²⁸ Villain, J., Bidaux, R., Carton, J.-P., and Conte, R., Order as an effect of disorder, *J. Phys. France* **41**, 1263 (1980).
 - ²⁹ G.-W. Chern and R. Moessner, Dipolar order by disorder in the classical heisenberg antiferromagnet on the kagome lattice, *Phys. Rev. Lett.* **110**, 077201 (2013).
 - ³⁰ M. E. Zhitomirsky, Field-induced transitions in a kagomé antiferromagnet, *Phys. Rev. Lett.* **88**, 057204 (2002).
 - ³¹ S. Schnabel and D. P. Landau, Fictitious excitations in the classical heisenberg antiferromagnet on the kagome lattice, *Phys. Rev. B* **86**, 014413 (2012).
 - ³² A. L. Chernyshev and M. E. Zhitomirsky, Quantum selection of order in an xxz antiferromagnet on a kagome lattice, *Phys. Rev. Lett.* **113**, 237202 (2014).
 - ³³ A. L. Chernyshev, Strong quantum effects in an almost classical antiferromagnet on a kagome lattice, *Phys. Rev. B* **92**, 094409 (2015).
 - ³⁴ E. F. Shender, V. B. Cherepanov, P. C. W. Holdsworth, and A. J. Berlinsky, Kagomé antiferromagnet with defects: Satisfaction, frustration, and spin folding in a random spin system, *Phys. Rev. Lett.* **70**, 3812 (1993).
 - ³⁵ M. E. Zhitomirsky, Octupolar ordering of classical kagome antiferromagnets in two and three dimensions, *Phys. Rev. B* **78**, 094423 (2008).
 - ³⁶ M. Taillefumier, J. Robert, C. L. Henley, R. Moessner, and B. Canals, Semiclassical spin dynamics of the antiferromagnetic heisenberg model on the kagome lattice, *Phys. Rev. B* **90**, 064419 (2014).

- ³⁷ C. L. Henley, Long-range order in the classical kagome antiferromagnet: Effective hamiltonian approach, *Phys. Rev. B* **80**, 180401 (2009).
- ³⁸ C. L. Henley, Ordering due to disorder in a frustrated vector antiferromagnet, *Phys. Rev. Lett.* **62**, 2056 (1989).
- ³⁹ C. Weber and F. Mila, Anticollinear magnetic order induced by impurities in the frustrated heisenberg model of pnictides, *Phys. Rev. B* **86**, 184432 (2012).
- ⁴⁰ T. Jolicoeur, E. Dagotto, E. Gagliano, and S. Bacci, Ground-state properties of the $S = 1/2$ heisenberg antiferromagnet on a triangular lattice, *Phys. Rev. B* **42**, 4800 (1990).
- ⁴¹ J. Fouet, P. Sindzingre, and C. Lhuillier, An investigation of the quantum j_1 - j_2 - j_3 model on the honeycomb lattice, *Eur. Phys. J. B* **20**, 241 (2001), 10.1007/s100510170273.
- ⁴² B. Schmidt and P. Thalmeier, Frustrated two dimensional quantum magnets, *Physics Reports* **703**, 1 (2017), frustrated two dimensional quantum magnets.
- ⁴³ M. V. Gvozdikova, P.-E. Melchy, and M. E. Zhitomirsky, Magnetic phase diagrams of classical triangular and kagome antiferromagnets, *Journal of Physics: Condensed Matter* **23**, 164209 (2011).
- ⁴⁴ G.-W. Chern, R. M. Fernandes, R. Nandkishore, and A. V. Chubukov, Broken translational symmetry in an emergent paramagnetic phase of graphene, *Phys. Rev. B* **86**, 115443 (2012).
- ⁴⁵ H. Kawamura and S. Miyashita, Phase transition of the heisenberg antiferromagnet on the triangular lattice in a magnetic field, *Journal of the Physical Society of Japan* **54**, 4530 (1985), <https://doi.org/10.1143/JPSJ.54.4530>.
- ⁴⁶ F. Y. Wu, The Potts model, *Rev. Mod. Phys.* **54**, 235 (1982).
- ⁴⁷ E. Bittner and W. Janke, Parallel-tempering cluster algorithm for computer simulations of critical phenomena, *Phys. Rev. E* **84**, 036701 (2011).
- ⁴⁸ A. M. Ferrenberg and R. H. Swendsen, New monte carlo technique for studying phase transitions, *Phys. Rev. Lett.* **61**, 2635 (1988).
- ⁴⁹ C. Weber, L. Capriotti, G. Misguich, F. Becca, M. Elhajal, and F. Mila, Ising transition driven by frustration in a 2d classical model with continuous symmetry, *Phys. Rev. Lett.* **91**, 177202 (2003).
- ⁵⁰ Henley, Christopher L., Ordering by disorder: Groundstate selection in fcc vector antiferromagnets, *Journal of Applied Physics* **61**, 39623964 (1987), doi: 10.1063/1.338570.
- ⁵¹ T. A. Tóth, A. M. Läuchli, F. Mila, and K. Penc, Three-sublattice ordering of the $su(3)$ heisenberg model of three-flavor fermions on the square and cubic lattices, *Phys. Rev. Lett.* **105**, 265301 (2010).
- ⁵² B. Bernu, L. Pierre, K. Essafi, and L. Messio, Effect of perturbations on the kagome $s = \frac{1}{2}$ antiferromagnet at all temperatures, *Phys. Rev. B* **101**, 140403 (2020).
- ⁵³ B. Bernu and G. Misguich, Specific heat and high-temperature series of lattice models: Interpolation scheme and examples on quantum spin systems in one and two dimensions, *Phys. Rev. B* **63**, 134409 (2001).
- ⁵⁴ B. Bernu and C. Lhuillier, Spin susceptibility of quantum magnets from high to low temperatures, *Phys. Rev. Lett.* **114**, 057201 (2015).
- ⁵⁵ J.-K. Kim and M. Troyer, Low Temperature Behavior and Crossovers of the Square Lattice Quantum Heisenberg Antiferromagnet, *Phys. Rev. Lett.* **80**, 2705 (1998).
- ⁵⁶ M. Calandra Buonaura and S. Sorella, Numerical study of the two-dimensional Heisenberg model using a Green function Monte Carlo technique with a fixed number of walkers, *Phys. Rev. B* **57**, 11446 (1998).
- ⁵⁷ B. Bernu and L. Messio, Detecting and characterizing a phase transition in spin systems using high temperature expansions.
- ⁵⁸ A. Zorko, F. Bert, A. Ozarowski, J. van Tol, D. Boldrin, A. S. Wills, and P. Mendels, Dzyaloshinsky-moriya interaction in vesignieite: A route to freezing in a quantum kagome antiferromagnet, *Phys. Rev. B* **88**, 144419 (2013).
- ⁵⁹ Villain, J., A magnetic analogue of stereoisomerism : application to helimagnetism in two dimensions, *J. Phys. France* **38**, 385 (1977).